

Recent developments in nuclear heating measurement methods inside the OSIRIS reactor

Hubert Carcreff, Laurent Salmon, Fadhel Malouch

▶ **To cite this version:**

Hubert Carcreff, Laurent Salmon, Fadhel Malouch. Recent developments in nuclear heating measurement methods inside the OSIRIS reactor. Nuclear Instruments and Methods in Physics Research Section A: Accelerators, Spectrometers, Detectors and Associated Equipment, 2019, 942, pp.162310. 10.1016/j.nima.2019.06.051 . cea-02535369

HAL Id: cea-02535369

https://cea.hal.science/cea-02535369

Submitted on 25 Oct 2021

HAL is a multi-disciplinary open access archive for the deposit and dissemination of scientific research documents, whether they are published or not. The documents may come from teaching and research institutions in France or abroad, or from public or private research centers.

L'archive ouverte pluridisciplinaire **HAL**, est destinée au dépôt et à la diffusion de documents scientifiques de niveau recherche, publiés ou non, émanant des établissements d'enseignement et de recherche français ou étrangers, des laboratoires publics ou privés.



Distributed under a Creative Commons Attribution - NonCommercial 4.0 International License

Version of Record: https://www.sciencedirect.com/science/article/pii/S0168900219308976
Manuscript_a851022702a4620486f285cacaccb416

NUCLEAR INSTRUMENTS & METHODS IN PHYSICS RESEARCH
Section A

Recent Developments in Nuclear Heating Measurement Methods inside the OSIRIS Reactor

Hubert Carcreff,[a] Laurent Salmon,[b] Fadhel Malouch[a]

[a]*DEN/DANS/DM2S/SERMA (CEN/Saclay), CEA-Université Paris-Saclay, F-91191 Gif sur Yvette Cedex, France*

[b]*DEN/DANS/DM2S/STMF (CEN/Saclay), CEA-Université Paris-Saclay, F-91191 Gif sur Yvette Cedex, France*

Elsevier use only: Received date here; revised date here; accepted date here

Abstract

Nuclear heating inside a Material Testing Reactor (MTR) needs to be known in order to design and to run irradiation experiments that have to fulfill target temperature constraints. To improve the incore nuclear heating knowledge of the French OSIRIS reactor operated by CEA, an innovative calorimetric system CALMOS (French acronym for CALorimètre Mobile OSiris) has been studied, manufactured and tested. This device can be inserted in any in-core experimental location. It is based on a mobile probe moving axially along the core height. First tests of this new probe, offering several ways for the heating evaluation, were performed in the reactor periphery. Then, two complete prototypes dedicated to incore measurements (calorimeter and the associated displacement system) were designed and tested during several reactor cycles. This paper presents a comprehensive analysis of all the results collected during the measurement campaigns carried out between 2013 and 2015 with these new

© 2019 published by Elsevier. This manuscript is made available under the CC BY NC user license
https://creativecommons.org/licenses/by-nc/4.0/

prototypes in various reactor conditions. A comparison is made with previous calorimeters and obtained advantages are emphasized. This new calorimeter has been designed as a real operational measurement system, well suited to characterize the radiation field inside an MTR reactor.

© 2001 Elsevier Science. All rights reserved

Keywords : Nuclear heating, differential calorimeter, incore measurements, OSIRIS reactor, mobile probe

---

1. Introduction

Nuclear heating inside an MTR reactor has to be known in order to predict sample temperatures during irradiation experiments and for safety reasons, to demonstrate that the highest temperature inside irradiation devices will not exceed material and thermohydraulic limits. Nuclear heating rate inside an MTR reactor is usually done using calorimeters. A calorimetric measurement in reactors can be done either with a sensor working in adiabatic mode (without heat exchange with the outside and measurement of temperatures in evolution), or with a sensor working in permanent mode (heat exchange with outside and stabilized temperatures in the sensor). Homemade calorimeters [1, 2, and 3], working in permanent mode, have been used for many years for the qualification of irradiation locations in the pool type MTR OSIRIS reactor.

Until recent years, OSIRIS calorimeters were designed with a pair of two aluminum cells, fixed onto the same aluminum base. Cells of each pair, both located at the same measurement level in the radiation field, are similar except that one contains a graphite sample while the other one has the corresponding volume filled with nitrogen (See Fig.1).

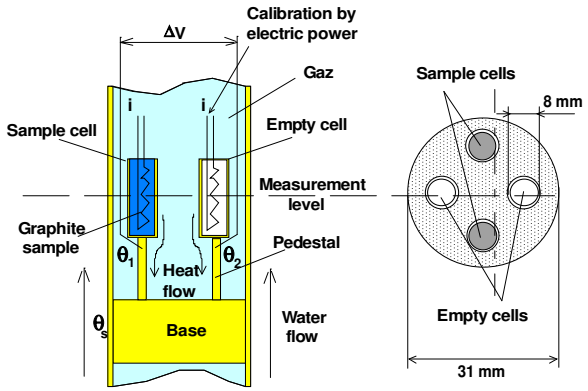


Fig.1. Static differential calorimeter previously used for heating measurements inside the OSIRIS reactor.

The two pairs of cells are diametrically opposed on the aluminum base to avoid any gradient effect in the calorimeter (heating radial distribution in the reactor). The whole structure is enclosed inside a tube in contact with the external water flow for heat removal. The pedestal, between the upper part of the cell and the base in contact with the external sleeve, plays the role of a thermal resistance through which the energy deposit inside the cell is evacuated towards the base.

The thermal flow difference between the two cells, proportional to the heating rate, is calculated thanks to temperature measurements and a calibration curve. This curve is done prior to any incore measurement, using a heater element located inside each cell and allows simulating the energy deposit by joule effect.

Note that the heating rate is written W/g (C) to emphasise the fact that it is relative to graphite. Devices for OSIRIS in-core measurements consisted of five different probes (each one made of four cells side by side, see cross section in Fig.1), piled-up along the core height leading to five measurement points, from which the heating profile curve was fitted. Inherent drawbacks of these calorimeters came essentially from the static nature of the technology. The heating distribution was plotted from only few measurement points, and the obtained distribution was restricted to the core height. In addition, each measurement point corresponded to a given calorimeter with its own calibration curve.

Furthermore, an accurate dimensioning of an experimental device requires as input data, the knowledge of the axial distribution of heating but not restricted to the core itself. In addition, one of the major problems of this static conception came from ageing effects under the radiation field, which can lead to difficulties for detecting the decrease of the calorimeter sensitivity under irradiation.

2. New concept of the nuclear heating measurement

To overcome inherent drawbacks of the previous technology, an innovative system has been studied, tested and run in the OSIRIS reactor. The key point of this new sensor is setting two cells (one empty and one equipped with the sample in which we evaluate the energy deposit), piled-up inside a same external sleeve, and then moving the whole in the core with the help of a displacement system [8]. Therefore, advantages of such a new probe, compared to the static one, are:

- To get a continuous heating profile instead of one deduced from only some points,
- To extend the axial measurement range above the core, where heating rates still remain high enough to be taken into account,
- To suppress entirely the ageing effect, because of a probe being in the radiation field only during measurement periods,
- To get all measurements by the same calorimeter, leading to a global consistency in the profile in terms of relatives values,
- To have a complete coaxial sensor design, allowing to avoid any asymmetric effect, facilitating any further modelling, therefore the comparison with calculation,
- To obtain pointwise measurements and to minimize any gradient effect thanks to a smaller size.

The new design is displayed in Fig 2. The upper cell contains a graphite sample, whereas the lower one is empty (reference cell). A gas gap (nitrogen) surrounds each cell. They are set on a base inserted inside a stainless external steel in contact with the water flow. A thermocouple (K type) is embedded on the top of each pedestal (“hot

temperature") whereas a second one is located on the external surface of the base or at the bottom of the pedestal ("cold temperature"). Two heating elements composed by a constantan wire embedded inside an alumina pearl, located inside the cells, allow the calibration. The energy deposit in the massive part of the cells is flowing through the pedestal and then through the external sleeve.

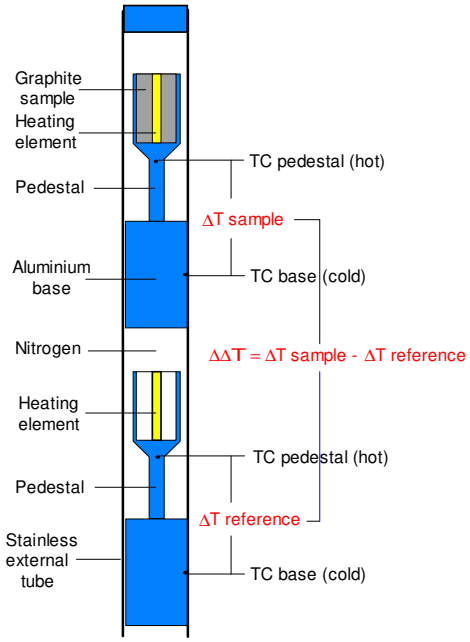


Fig.2. CALMOS design with its two piled-up cells configuration.

The temperature difference "ΔT sample" (see Fig.2) is proportional to the energy deposit both in graphite and the cell structure, whereas "ΔT reference" is proportional to the only deposit in the empty cell structure. Therefore, in first approximation, if cells are identical, the difference "ΔT sample - ΔT reference" quantity (ΔΔT) is proportional to the energy deposit inside the only graphite sample. This new nuclear heating measurement method has been patented [7].

As both cells are superimposed in a same envelope (Fig. 2), measurements are performed in two steps at each altitude in the core, by moving the probe in the radiation field.

Along this R&D program, different phases followed each other, before reaching a complete device, which allows incore measurements up to the nominal power:

- Two mock-ups have been successively manufactured and tested in the reactor periphery, up to a 2 W/g (C) limited heating rate, to check the probe manufacturing and the measurement protocol,
- A first complete equipment CALMOS-1 (probe associated to a displacement system) has been tested inside the core in the 2011-2013 period (during 8 cycles) [9, 16, 23] which allowed to have a significant feedback, to highlight the required improvements on this first prototype so as to reach a real operational measuring system,
- Finally, the CALMOS-2 device [28], has been manufactured, calibrated and tested during the last 3 cycles in 2015. It is the updated version which can be considered as a qualified measurement device for incore measurements. The automatic cell mobility, with a specific software through a Human Machine Interface (HMI) allowed highlighting the different possibilities of this new sensor.

This paper relates the entire R&D program, from the conception, the modelling, the manufacturing, the calibration and the qualification phase inside the core. Thanks to all results collected during the measurement campaigns, a comprehensive analysis is presented.

However, for detailing the cell configuration, the last upgraded CALMOS-2 version is taken as reference.

3. Calibration of the calorimeter

Prior to any measurement, a calibration is performed in out of pile conditions [9]. Firstly, the calorimeter behavior is checked in natural convection, directly into the pool of the reactor. A first calibration curve is done, and the linearity is verified.

Secondly, we check that the calibration coefficient remains unchanged when the probe, set on its displacement device, is placed on a bench simulating real thermohydraulic conditions. The slope of each cell (°C/W) is measured.

The calibration procedure requires applying different electric powers to heaters (the constantan wire used for heaters limits the applied power to around 5W), and to measure pedestal and base temperatures after stabilization. If we consider that the heat transfer is only made by conduction through the pedestal, and applying the conduction law to calculate ΔT between hot and cold thermocouples (see Fig 2), a K calibration coefficient for the calorimeter is defined ($W.g^{-1}.°C^{-1}$) by:

$$K = \frac{1}{M_E P_E + m_V \,.\, (P_E - P_V)} \qquad (1)$$

Where P_E and P_V are the slopes (°C/W) of sample and reference cells, M_E the graphite sample mass and m_V the total mass of structure (aluminum + heater) above the hot point ("hot temperature"). The term $m_V (P_E - P_V)$ relates to the difference of thermal responses between cells, due to inevitable slight manufacturing differences, and secondly to take into account that bases of the two cells are not exactly in the same environment. If sample and reference cells are in a same radiation field, the total heating rate E_T is given by:

$$E_T = K_C (E_T).K \,.\, \Delta\Delta T \qquad (2)$$

where ΔΔT is defined as ΔΔT = ΔT sample – ΔT reference and $K_C(E_T)$ to the nonlinearity coefficient. This latter depends of heat leakages by radiation or conduction in the gas and, on the other hand, on the conductivity dependence of aluminum with temperature. Lower are temperatures reached in the cell, better is the linearity [11]. $K_C(T)$ has been evaluated both by using the finite element model and thanks to measurements up to 13 $W.g^{-1}$.

4. Possible measurement ways with the new sensor

4.1 Use of the K coefficient from calibration

Once the probe calibrated, the measurement in the radiation field is performed in two steps.

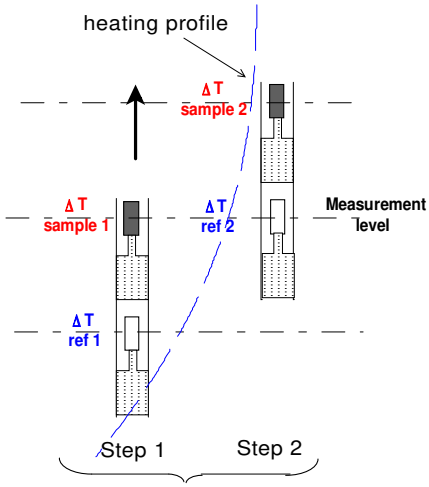


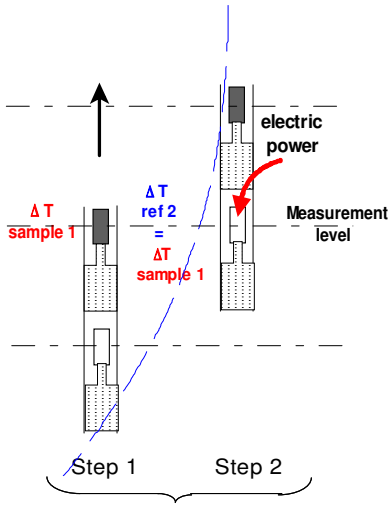
Fig.3. Procedure for the nuclear heating measurement in the radiation field of the reactor core.

Starting from a given static position in the radiation field, temperatures of the sample cell are recorded. Then, taking advantage of the moving system, the whole calorimeter is shifted (moved up or down), in such way that the reference cell position matches with the previous sample cell location. Temperatures of the reference cell are recorded. Then, heating is deduced using (2) when cells are at the same level. As shown in Fig.3 the displacement step by step allows drawing the entire heating profile. Note that the elevation step can be a subdivision of the distance between cells to draw the heating profile as finely as required.

4.2 Use of the "zero method"

In addition to use the calibration phase, advantage of such a calorimetric sensor is offering another nuclear heating measurement so called the "zero method". Fig.4 illustrates the measurement of heating through the "zero method". The two cells being at the same altitude in the core, the nuclear energy deposit inside the sample can be

155 evaluated by adjusting an electrical power in the reference cell heater (simulating the energy deposit in the sample by
156 radiation) so as to equalize ΔT sample and ΔT reference.



157
158
159 Fig. 4. The two cells being located at the same core level, the current intensity is adjusted inside the reference cell heater until to cancel the quantity
160 "$\Delta T_{Reference} - \Delta T_{Sample}$".
161
162 Then, the heating rate E_T in the sample is deduced from:
163
164 $$E_T = \frac{W_e}{M_E} . K_0 \qquad (3)$$
165
166 Where *We* is the dissipated electric power (W) in the reference cell and M_E the graphite sample mass (g). We note
167 that K_0 is equal to 1 if both slopes are identical. As there are inherent small differences of thermal transfer capabilities
168 (slopes in °C.W^{-1}) between the two cells, a K_0 correction factor is needed (the temperatures equilibrium is made with
169 the reference cell):
170

171
$$K_0 = \frac{\frac{P_V}{P_E}}{1 - \frac{m_V}{M_E} \cdot \left(\frac{P_V}{P_E} - 1\right)} \qquad (4)$$

172

173 With P_V an P_E the slopes in °C/W for the reference and the sample cells respectively, m_V the mass of the cell
174 corresponding to the part located the "hot" thermocouple and M_E the sample mass.

175 The "zero method" is considered as the most reliable measurement because it is performed without using the
176 preliminary calibration. To improve the reliability of this method, two major improvements have been implemented in
177 the last upgraded CALMOS-2 version [28] (Fig.5).

178

179 Position of thermocouples: Cells have not the same thermal transfer capability (slope in $°C.W^{-1}$), so the lower the
180 difference is, the lower the K_0 influence in equation (3) is. The best way to tend K_0 to unity is to limit the thermal
181 resistance between the two measurement points to the only Aluminum cylinder (pedestal, see Figs.5 and 6). The effect
182 is significant. The slopes discrepancy in the last version has been reduced to 0.3 % [28]. The K_0 correction coefficient
183 is now close to 0.99 (0.955 for CALMOS-1). By that way, performing a measurement using the zero method is nearly
184 independent of slopes measurement, i.e of the calibration phase.

185 Power measurement: In addition to considering that the heat dissipation inside the heater element is fully
186 representative of the energy deposit by nuclear heating, we need also to be confident on the power measurement
187 during the equilibrium phase.

188 Calculations of the *We* energy deposit assume that the effective resistance r of the heater element is well known,
189 and more importantly, that r does not change with ageing, temperature or irradiation conditions. Therefore, to measure
190 more accurately the energy deposit by joule effect, and to avoid any assumption about the resistance evolution in the
191 reference cell, this latter is equipped with a 4-wire element heater element, two wires for the intensity and two for the
192 voltage measurement (Figs. 5, 6).

193

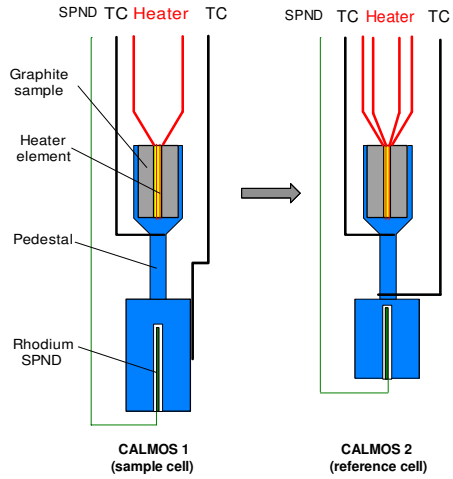


Fig.5. Evolution of thermocouples locations and heater wiring to improve the "zero method" accuracy.

Therefore, the applied electric power to the heater is measured by $W_e = U\ I$ (U the voltage, I the intensity) instead of $We = r\ I^2$. Such implementation led to one of the major difficulty in the manufacturing, because the whole wiring has to be inserted inside an overall 17mm diameter, each wire insulated from each other.



Fig.6. CALMOS-2 details: upgraded position of thermocouples located at the top and bottom of the pedestal (left), and implementation of a 4-wire resistance inside the reference cell of the calorimeter (right).

5. Numerical modeling of the sensor

5.1 Modelling of the sensor

Temperatures inside the probe were required prior experiments for safety reasons. These temperatures were calculated using a Finite Element model of the sensor. This model was built using the FE CAST3M calculation code [24]. The whole probe was modeled using an axisymmetric description. Only very few simplifications were made on the cell description. Main ones are the suppression of the wires connecting the cells to the outside and the suppression of the rhodium SPND inside the lower base. The upper part of the device (sealed passage and above) was somewhat simplified since its plays only a secondary role on the measurement process. Fig. 7 displays the sensor meshing, to be compared with Fig. 9.

For practical reason, a small gap had to exist between each cell base and the external sleeve. It allows inserting the cells inside the sleeve during the sensor manufacturing. This mechanical clearance was determined from dimensional measurements. It is very small (24 micrometers at ambient temperature) but had to be considered in the FE model to get accurate results.

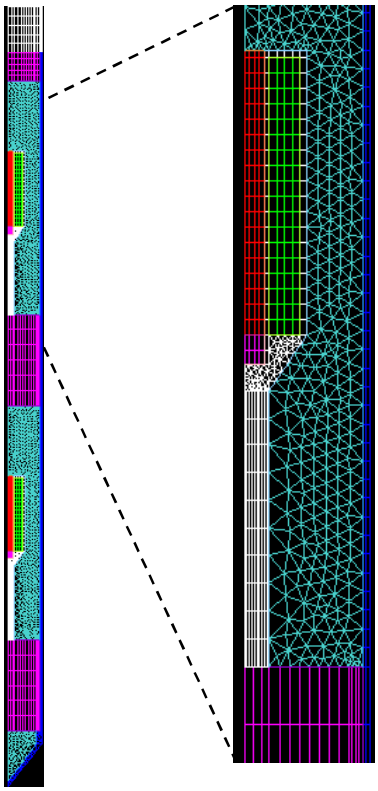


Fig.7. Meshing of the whole calorimeter (left) with focus on the sample cell (right)

Indeed, this gap is filled with nitrogen, which has a very low thermal conductivity (0.026 $W.m^{-1}K^{-1}$ at 27°C). It insulates the cells from the outside and has an important effect on absolute temperatures inside the cells. In the FE model, the gap width was set to depend on temperatures since thermal dilation coefficients of aluminum (25 x 10^{-6} K^{-1} at 25 °C) and stainless steel (16.5 x 10^{-6} K^{-1} at 25 °C) are different. In order to avoid micrometer size meshes (gap between the external surface of aluminum bases and the internal surface of the steel sleeve) aside to millimeter ones (steel sleeve), a local apparent conductivity of the stainless steel located in front of the gap is calculated (postulating a two cylinder serial configuration) and used at different steps of the FE simulation.

Physical characteristics of the different materials play a key role on the obtained results. Values of heat capacity (Cp), thermal conductivity (λ), coefficient of expansion (α), volumetric mass (ρ) and their dependence with temperature have been taken in literature. As thermal characteristics of aluminum AW1050 have a significant impact on temperatures inside the cells, a specific determination by measurements was ordered to a metrology specialized laboratory [27]. Except for the volumetric mass which is considered constant at 2670 kg.m^{-3}, other data were used in the last version of the FE model [25, 26]. They are summed up in Table 1.

T (°C)	ρ (kg.m^{-3})	Cp (J.K^{-1}.kg^{-1})	λ (W.m^{-1}K^{-1})
24	2684	886	
100	2668	939	24.8
200	2648	982	25.2
300	2627	1018	25.6
400	2605	1059	26.3
500	2582	1109	27.2

Table 1. Thermal characteristics of the aluminum AW1050.

In the FE calculation, the thermal power is injected in the device as a specific power (W.g^{-1}). The same specific power is used for all different components of the calorimetric cell regardless the atomic number of their constituting material. This assumption was considered as appropriate considering previous experiments made inside the OSIRIS reactor.

Velocity of water around the probe was measured on an experimental bench before putting the measurement device in real conditions in the reactor. This velocity value was used to calculate the Reynolds number and then the thermal flux exchanged between the probe and the pool using the Dittus Boelter correlation. Water

temperature inside the device (internal flow in the displacement system, see Fig. 18) was measured by dedicated thermocouples.

On the other hand, a polished mirror is placed around the cell in the design. That allows to limit heat losses by radiation by adjusting in the cell the internal walls emissivity. Nevertheless, this thermal screen is not perfect. A sensitivity study performed on the CALMOS-1 cell (very similar to CALMOS-2), using an aluminum surface emissivity of $\varepsilon = 0.05$ $W.m^{-1}K^{-1}$ and $\varepsilon = 0.01$ $W.m^{-1}K^{-1}$, led to a 1.4 % difference on the calculated heating rate E_T (temperature of the graphite is roughly 500 °C). As it is very difficult to determine which coefficient to use, and as the effect remains small, we chose not to take into account radiative thermal losses in the CALMOS-2 model. Fig. 8 shows an example of temperature map obtained for in pile conditions when a 13 $W.g^{-1}$ heating rate is applied in the FE model.

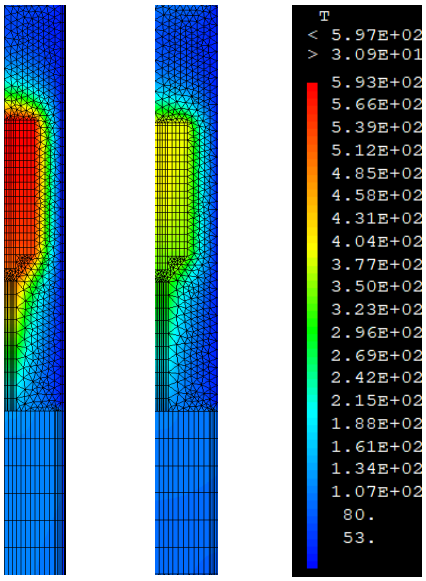


Fig. 8. Example of temperature distribution inside the cells obtained for 13 W/g with FE modelling (left: sample cell; middle: reference cell; right: temperature scale).

5.2 Comparison between calculations and measurements

The first comparison is made on experimental results obtained during the calibration process of the probe. As the simulation is concerned, the Joule electric power is injected as a volumetric power applied inside the alumina pearl volume (element heater). Water temperature surrounding the probe is measured during the experiment. Fig.13 shows that calculated results are in very good agreement with experimental data. However, the range of power variation is limited because the total energy applied to the element heater (4.5 W in Fig.13) corresponds roughly to a simulated 5 $W.g^{-1}$ heating rate.

On the other hand, comparisons were made with measurements performed in real OSIRIS incore conditions. Results agree quite well for low to medium nuclear powers. For highest values, some discrepancies appear leading to a nonlinear behavior between the input nuclear power and the calculated one. One part of these discrepancies could come from the behavior difference between both cells regarding the thermal radiative flux (heat losses by radiation), despite the use of mirror-polished screens located around the cells. Another source of nonlinearity could come from the non-symmetric axial environment of both cells. We tried in other papers to calculate the $Kc(E_T)$ (2) factor in order to correct these non-linearity effects. Nevertheless, even if interesting results are obtained, it is difficult to assert the value and could not confirm the non-linearity evolution, which has been experimentally found and presented in Figs. 23 and 36.

6. Optimized characteristics

Fig.9 shows a cross section of the final CALMOS-2 calorimetric probe. Taking into account thermohydraulic conditions, mechanical constraints, and incore conditions requirements, optimized values for main dimensions are [28]:

- Base: AW1050 aluminum, 17 mm in diameter, 25 mm height,
- Pedestal: aluminum, 3.8 mm in diameter, 20 mm height, 20 mm between TCs locations,
- Sample: graphite
- Cell upper part: sample weight 1.432 g, 8 mm in diameter, 20 mm height,
- Mass of the cell upper part 1.621 g,
- External sleeve: stainless steel 0.5 mm thick, overall height 210 mm,
- Internal gas: N_2, capsule pressure 1.5 bar,
- Half-screens: stainless steel, 0.2 mm thick,
- Heater: constantan wire, 0.25 mm in diameter, resistance 1.8 Ω, 4-wire resistance for the reference cell, 2 A maximum,
- Distance between cells: 88 mm,
- SPND: Rhodium emitter 0.5 mm in diameter, 10 mm length.

The picture in Fig. 10 illustrates the preliminary assembly of both cells, before their insertion inside the external sheath, with upper polished half-screens not assembled yet.

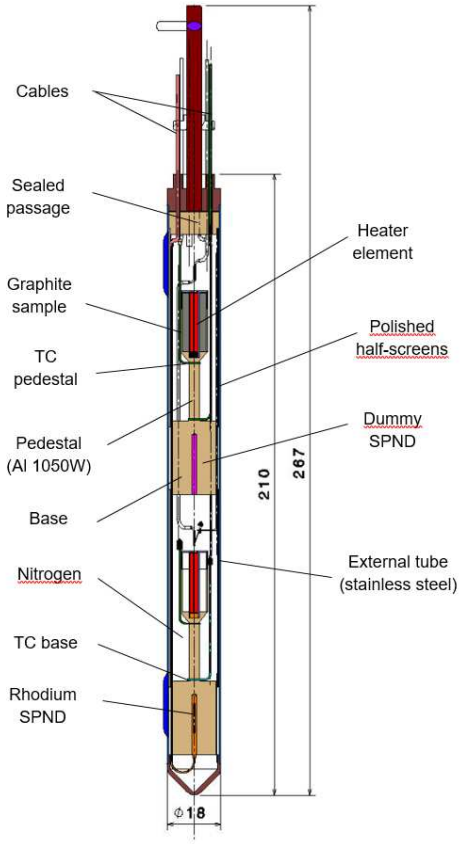


Fig.9. Overall cross section of final design of the calorimetric cell (CALMOS-2 configuration).

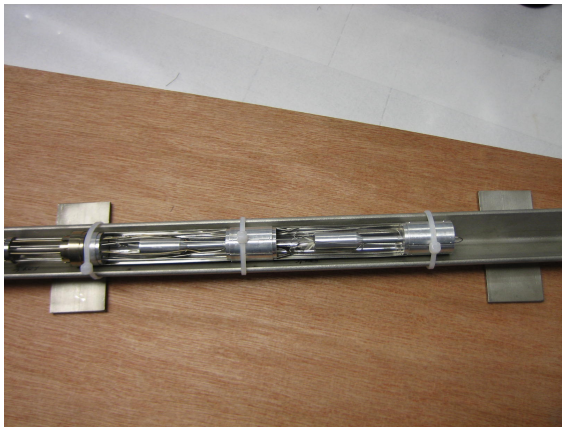


Fig.10. Intermediate step in the CALMOS-2 manufacturing. The two cells are in a temporary guide and thermocouples are put into place, but polished half-screens are not assembled yet.

7. Measurement of the thermal neutron flux

Measurement of the conventional thermal neutron flux (flux normalized to the 2200 m/s neutron speed) is made thanks to a Rhodium SPND, especially designed to fit the calorimeter cell geometry. This SPND is similar in terms of material and cross section to the standard one used for many years in OSIRIS reactor, but with a rhodium emitter length reduced to only 10 mm whereas the standard one is 50 mm. The total length is around 20 mm allowing its implementation inside the aluminum cell base. In CALMOS-1 the SPND is embedded inside the upper cell (around mid-height of the sensor) whereas for the last version it is embedded inside the lower cell. This change allows extending the accessible length by more than 100 mm in the core axis with CALMOS-2 (Fig. 21). The lowest accessible altitude for the first version is -191 mm/core mid-place against -294 mm for the updated one. This improvement is significant with regard to a total fissile height of 640 mm.

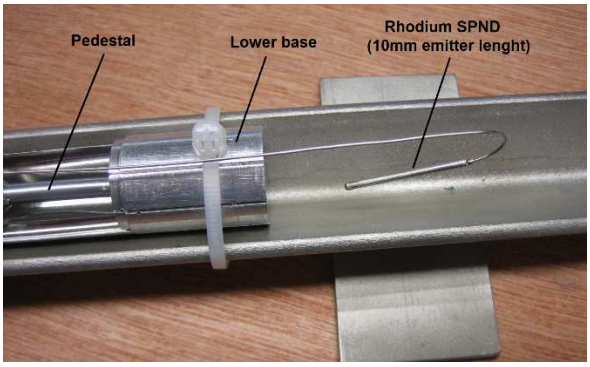


Fig.11. CALMOS-2: Shaping and introduction of the specific SPND (rhodium emitter 0.5mm in diameter, 10mm length) inside the lower base (overall length 20mm).

The rhodium emitter offers a good sensitivity, but the capture reaction $^{103}Rh(n, \gamma)^{104m}Rh$ used for establishing the signal (current intensity) has a response both in thermal and epithermal ranges. The thermal flux measurement needs to be made along the entire mechanical stroke, from -160 mm to +960 mm/core mid-plane. However, the neutron spectrum varies a lot along this range and needs to be calculated for deducing the thermal flux from the delivered intensity.

The epithermal index (epithermal neutron flux/thermal neutron flux) characterizes the spectrum for energies in the thermal range and is used to process the SPND signal. It is calculated inside the cell with the TRIPOLI-4® Monte Carlo code at the precise location of the SPND and for any accessible altitude in the core [12, 21]. Fig 12 shows the evolution of this index calculated inside the 64 experimental location. Note that the index decreases sharply at the fuel-moderator transition to become ten times lower in water. The relative contribution to the total current of the SPND due to the epithermal contribution is around 5 % in the upper part of the core (in full moderator) whereas it can reach around 48 % at the core mid-plane. This shows that the epithermal index knowledge, all along the CALMOS mechanical stroke, is of major importance for using a Rhodium SPND located inside the calorimetric cell.

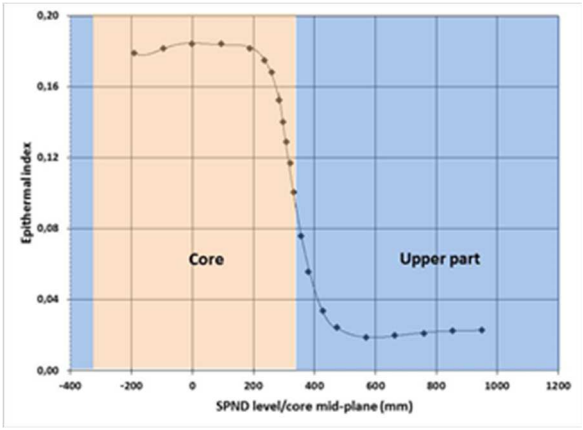


Fig.12. Calculated epithermal index (epithermal neutron flux/thermal neutron flux) evolution in the 64 experimental location along the total mechanical stroke of the calorimeter. The associated uncertainty is less than 1 %.

8. Results of the calibration

The calibration phase (see chapter 3) is performed in no radiation conditions and in both natural and forced convection. The purpose is to determine not only the K calibration coefficient (1), linking the $\Delta\Delta T$ measurement to the nuclear heating rate E_T, but also the time constant of the calorimeter, i.e the time necessary to get a stabilized temperature map inside the calorimetric probe. During the calibration following key points are measured:

- The cell slopes (°C/W) from which K is deduced and the slopes linearity up to a 5 W electric power,
- The independence of both cells. The electrical power is applied in heaters separately or simultaneously to both reference and sample cells. It is essential to check that there is no influence of cells on each other,
- The validation of the K coefficient in forced convection conditions,
- The time constant of the calorimeter, defined in this experiment as the time required to reach 99 % of the stabilized signal after a transient. That drives the total time required to draw heating profiles in the reactor.

Fig. 13 shows the result of the slope measurement of the CALMOS-2 sample cell, illustrating the excellent linearity up to a 4.7 W applied to the heater element. In the same figure is plotted also the determination by calculation performed with the CAST3M finite element model (see chapter 5). The C/M ratio is less than 0.15 %. However, for this low level of power, the whole energy deposit in the upper part of the cell is entirely evacuated by conduction through the pedestal. We do not have any heat leakage (radiation, conduction in gas) to take into account in the modelling.

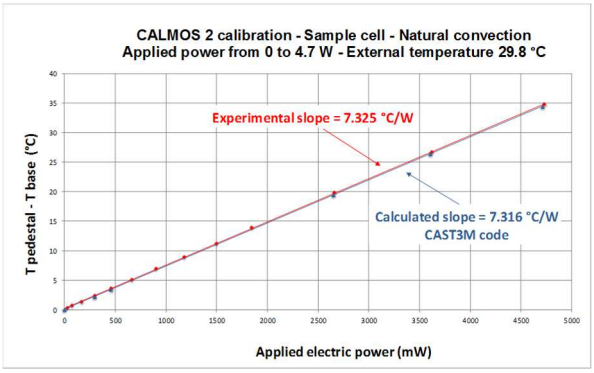


Fig.13. Experimental determination of the sample cell slope of the CALMOS-2 probe in natural convection.

Table 1 gathers all results of slopes determination and permits to illustrate that:

- The slope of the sample cell is very close to the reference one. That demonstrates the manufacturing accuracy and also, the weak influence of unavoidable discrepancies in the thermocouples setting along each pedestal,
- The two different thermohydraulic conditions lead to a maximum of 1.8 % dispersion on the slope determination (case of reference cell, separated heating). Such a discrepancy is included in measurement uncertainties,
- The heating mode (separated or simultaneous) has no influence on slopes determination, demonstrating that there is no significant thermal influence between both cells. It is a critical point to validate the “zero method” protocol, at least up to a 5 W applied electric power,
- Among all configurations, the dispersion is less than 1.3 % for the sample cell against 1.9% for the reference one.

To check results obtained in natural convection, tests performed on the hydraulic bench were limited to only 2 applied electric powers covering the whole 5 W energy range. Therefore, the final K calibration coefficient,

421 retained for the CALMOS-2 exploitation, is the average of the two results obtained in separated and simultaneous
422 heating, and in natural convection.
423

Thermo hydraulic conditions	Natural convection (≈ 30 °C)		Forced convection (≈ 40 °C - 1.24 $m^{3.-1}$)	
Heating mode	Sep.	Sim.	Sep.	Sim.
P_S slope ($°C.W^{-1}$)	7.325	7.337	7.418	7.388
P_R slope ($°C.W^{-1}$)	7.301	7.294	7.432	7.344
K ($W.g^{-1}.°C^{-1}$)	0.0950	0.0945	0.0943	0.0939
K Retained value ($W.g^{-1}.°C^{-1}$)	**0.0948**			

424
425 Table 2. Experimental results of CALMOS-2 calibration.
426
427 The second major parameter is the calorimeter response time (or time constant), which is an important
428 criterion. It must be taken into account to define, before starting measurements, the allowed definition (number of
429 steps) compatible to the possible modification of the radiation field (control rods movement) during the expected
430 duration of the total scanning. As this time depends on cooling conditions, it is measured in natural and forced
431 convection [13, 19]. Preliminary tests, performed on the two mock-ups (illustrated in Fig. 14), showed that the
432 response time measured during a temperature rise is slightly higher to the time measured during a decrease
433 (roughly 15 s over a 250 s total time). On the other hand, in natural convection, the presence of the external

sheath (required for a calorimeter in incore conditions) leads to increase the response time (roughly 8 s over a 250 s total time). Indeed, when the calorimeter is inside its external sheath (situation illustrated in Fig.18), the heat extraction is ensured by the only 1.5 mm static water gap surrounding the calorimeter (in natural convection). Such situation occurs when primary pumps stop (no primary flow).

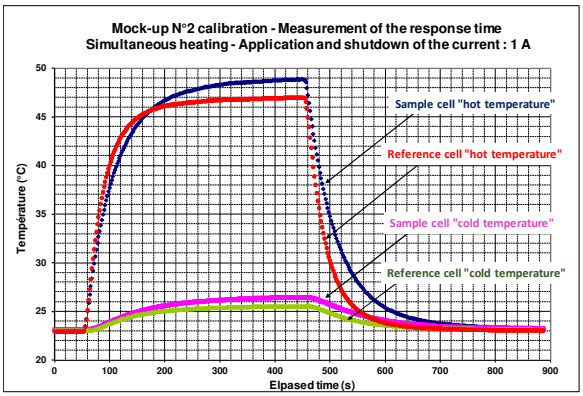


Fig.14. Measurement of the response time on the mock-up N°2. Evolution of temperatures during a power transient, after application and shutdown of a 1 A intensity in both element heaters.

Therefore, the measurement of the time constant of calorimetric cells, when set on their displacement systems (CALMOS-1 and 2), are performed by recording the temperature decrease, first to measure the longest time constant of the whole cell, and secondly to avoid any constraint involved by applying a too much sharp step of power to element heaters. To perform this measurement, a 0.8 A is applied to both heaters until thermal equilibrium. After turning off the current, temperatures are recorded (example in Fig. 15). The analysis of Figs. 14 and 15 shows that the time response of the sample cell is longer than the reference one, due to the additional thermal inertia induced by the graphite. Table 2 refers to results obtained in natural and forced convection for the CALMOS-1 calorimeter, similar to the last version. It gathers measured values corresponding to times required to reach 99 % of the stabilized signal. Obviously, it shows a significant gain of time response when using the OSIRIS forced convection.

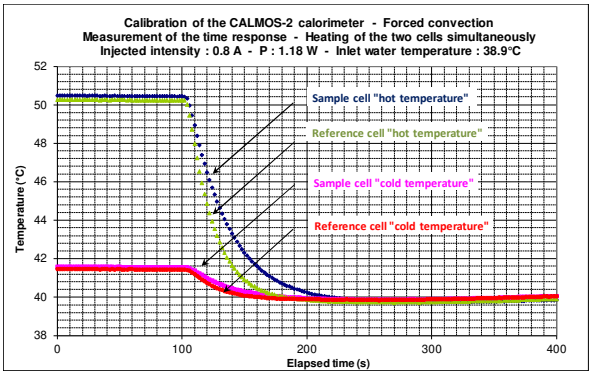


Fig.15. Measurement of the CALMOS-2 calorimeter response time by a decreasing transient.

For the OSIRIS thermohydraulic conditions, the response time of the sample cell is close to 2 min 30 s. That value governs the total time required to reach the temperatures stabilization in the whole probe, after any change of position in the reactor radiation field. Table 2 shows also that, when the sensor is used inside the core but without primary flow (measurement at very low reactor power or follow-up of the residual power) the waiting time to make a heating measurement requires a total time at least 30 % longer.

Conditions	Natural convection	Forced convection	Discrepancy (N-F/N)
Sample cell	210 s	**155 s**	-26%
Reference cell	150 s	**90 s**	-40%

Table 3. Experimental results of the response time measurement on the CALMOS-1 calorimeter.

Note also that using the AW1050 Aluminum alloy for the cells allowed reducing the response time due to its higher thermal conductivity. (230 $W.m^{-1}.K^{-1}$ against 130 $W.m^{-1}.K^{-1}$ for the AW 5754 alloy at around 100 °C)[26, 27].

9. Generalities about the OSIRIS reactor

OSIRIS was a pool type light water reactor with an open core. The core itself is a compact unit, with an horizontal section of 60 cm × 70 cm and a height of 70 cm. The core housing contains a rack of 56 cells. This rack is loaded with 38 standard fuel elements, 6 control elements and up to 7 beryllium elements. At least two experimental locations (22 and 26) are dedicated to radioisotopes production for medical application (MOLY devices). Remaining locations (24, 44 and 64) receive experiments, and are equipped with water boxes (82 mm x 82 mm) which can contain up to 4 experiment rigs (37 mm in diameter) (see Fig. 16).

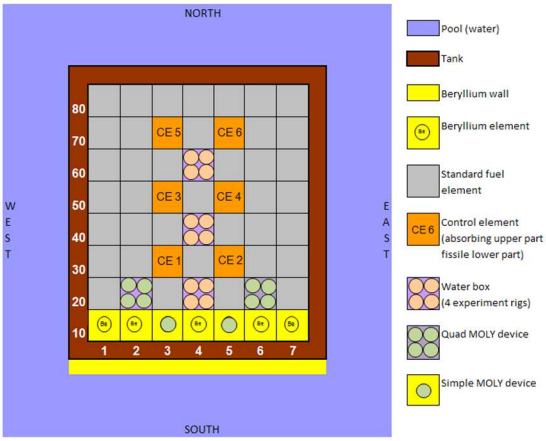


Fig.16. Horizontal cross-section of the OSIRIS core

Purpose of the CALMOS device is making measurements in 24, 44 and 64 locations. The core configuration is such that the heating level is higher when we go from the south to the north, i.e 24 then 44 and finally 64. All measurements carried out from 2013 to 2015 with CALMOS-1 and CALMOS-2, and detailed hereafter, were

carried out in various core conditions (start-up, steady state, shutdown, core loading, rods positions and configuration of experimental devices).

10. Description of the displacement system

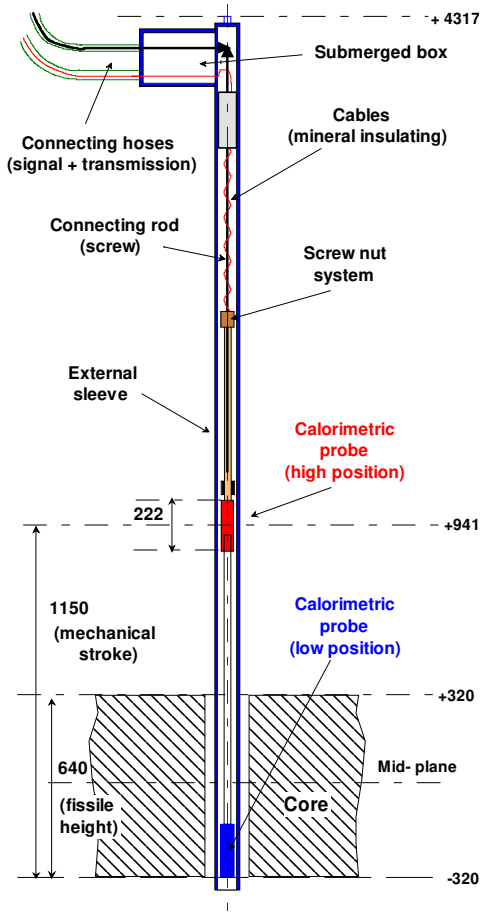
The study of the displacement system, allowing the movement of the calorimetric cell inside the core is as important as the development of the calorimetric cell itself. This device needs to answer not only to conditions for performing a measurement inside the core, but also as a standard incore experiment, to meet all conditions in terms of reactor safety.

Main purpose of this paper is not detailing this part of the R&D program. However, a short description is given hereafter to illustrate the working mode, objectives, limits, and difficulties for moving a probe inside an experimental reactor. The challenge to cope with was to get incore axial distributions while preserving permanently both same measurement conditions and the required safety margins.

The complete device is in two parts: the calorimetric cell and the displacement system. The device is set inside the core before reactor start-up, and taken out after the end of the cycle. It is inserted into a water box (reactor equipment) and inside one of the four available experimental locations (Fig. 17).

The displacement system is mainly made of an external sleeve (composed of aluminum and stainless steel) inside which the calorimetric probe moves along a 1150 mm mechanical stroke corresponding to the core fissile height and 510 mm above fuel elements, as shown in Fig. 17. Inside the connection box (link between out of pile and in pile cables), placed above the pool surface 7 m away from the upper part of the displacement system (not visible on Fig. 17), an electric engine rotates a cable inside its own sheath (mechanical transmission). This rotation movement is transferred from the connection box to the submerged box. Inside this latter, located at the top of the displacement system (around 4 m above the core mid-plane), a mechanical connection is made thanks to a gearing set between the cable and a connecting rod, itself linked to the mobile equipment. From the bottom to the top, the mobile equipment of CALMOS is made of the probe itself linked to the insertion tubes, themselves connected to a screw nut system, itself connected to the connecting rod. By rotation on its axis, the cable moves

509 the whole vertically inside the external sheath. Two flexible hoses connect the submerged box to the upper
510 connection box (Fig. 8), the first being dedicated to the mechanical transmission (cable in rotation) and the
511 second one to the cell signals (thermocouples and rhodium SPND).
512



513
514 Fig.17. Main components of the displacement system equipped with the calorimetric probe (in blue and red according to the position).
515
516 Main requirements for the displacement system are:
517

- Ensuring a relevant heating measurement, as close as possible to the actual heating inside a standard experiment used for material irradiation. The material composition on the 37 mm cross section (water + external sleeve + calorimeter) must be as close as possible to the standard experimental capsule,
- Ensuring a displacement range as large as possible; the total mechanical stroke is 1150 mm corresponding to the fissile height of fuel elements and a sufficient height above,
- Offering a rest position for the calorimeter. The highest altitude of the cell is around 900 mm with regard to the core mid-plane (see Fig. 17). At this position, the estimated residual heating rate is less than 30 $mW.g^{-1}$ and the thermal neutron flux level less than 10^{11} $n.cm^{-2}.s^{-1}$, avoiding any significant ageing effect on the probe,
- Centring the calorimetric cell (18 mm in diameter) along the vertical axis which has a 37 mm internal diameter,
- Ensuring the role of guide and housing for all the cables required for measuring the signals. That was the major difficulty in the design. The cables, with mineral insulation and stainless steel sheath (1mm in diameter), are twisted together in a spring shape so as to accommodate the 1150 mm total stroke by successive stretching and compression,
- Ensuring appropriate cooling conditions of the probe whatever its altitude in the core. If ΔT sample and ΔT reference temperature differences do not depend on the water cooling temperature and the water flow (but only to the heating rate), absolute temperatures reached inside the cells depend directly on cooling conditions. The hottest allowed temperature inside the cell structure is fixed to 500 °C in order to keep a sufficient margin against aluminum melting [26]. Therefore, it is essential to ensure a good cooling. The design allows to cool both the external sheath (external flow) and the mobile equipment (internal flow). This internal cooling flow enters the sheath tube through its base (located under the fissile height of the core) and exits through several holes located above the probe rest position (Fig. 15). In nominal conditions, the internal flow is 1.35 $m^{3}.h^{-1}$ (measured on a specific hydraulic bench representative of OSIRIS conditions) corresponding to a 3.2 $m.s^{-1}$ linear speed around the probe. The cooling flow

variation does not exceed 12 % for a probe running from the top to the bottom of the total mechanical stroke.

In addition, the system has to meet the safety requirements in terms of reactivity. The insertion of the mobile equipment in the sleeve changes the local composition of the water box as the descent progresses, involving a reactivity effect on the core.

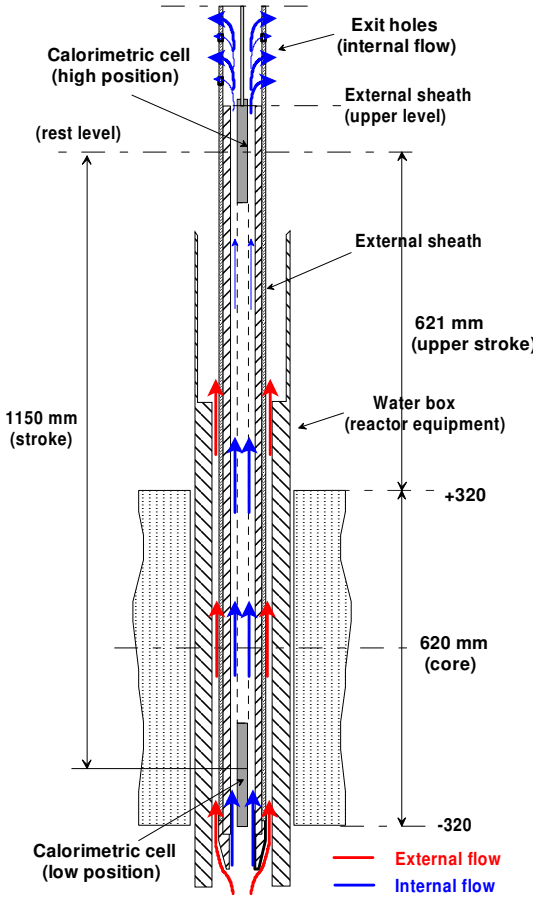


Fig.18. Cooling water flows inside the CALMOS device, when located inside an experimental location of the OSIRIS core.

Therefore, this effect has to be evaluated to check that, first, it does not disturb reactor operation in terms of safety and, secondly, that the control rods movement for compensating this effect does not modify the radiation field we are measuring. Results of this study are:

- Calculation showed that, whatever the experimental location, the reactivity effect induced by the total insertion of the mobile equipment does not exceed 70 pcm. Such low impact complies with OSIRIS safety requirements,
- To avoid any disturbance on the reactor, the vertical speed of the probe during the insertion phase is limited to 5 $mm.s^{-1}$, leading to a reactivity effect less than 0.5 $pcm.s^{-1}$. In practice, to add a margin, the vertical speed was further limited to 1 $mm.s^{-1}$ when the cell goes through the fissile height of the core. As a result, no disturbance on the reactor operation was noticed during measurement campaigns,
- The double monitoring of the radiation field by two devices located side-by-side in the same 64 location (detailed in § 18), showed that the disturbance led by one calorimeter progression inside its own sheath, does not involve significant changes in the close vicinity i.e in adjacent locations in the same water box.

11. Generalities about incore measurement campaigns

For each CALMOS device, a comprehensive measurement campaign has been carried out inside the core. The CALMOS-1 measurement campaign lasted 10 OSIRIS cycles, corresponding to 8 cycles for the prototype itself and 2 additional ones for the comparison with the updated CALMOS-2 version. Taking into account the scheduled final shutdown of the reactor, planned at the end of 2015, the development, manufacturing, calibration and all the tests of this last configuration had to be done during the only last 3 cycles of OSIRIS reactor. To qualify CALMOS devices, the following kind of tests were carried out:

- Three incore locations, 24, 44 and 64 (in ascending order of heating rate), were measured. We remind that a single location can be investigated per cycle,
- For the only device CALMOS-2, 21 complete automatic scanning were performed,
- Follow-up of the reactor start-up with the probe located at the core mid-plane,

- Follow-up of the residual power decay with the probe located at the core mid-plane,
- Measurement of the mutual influence, in terms of heating and thermal flux, between both devices when they are placed side-by-side in a same location,
- Comparison of CALMOS and MEREVER devices in terms of thermal neutron flux,
- Measurement of the reactivity effect consequently to the insertion of the mobile equipment inside the core,
- Influence of the probe displacement speed on the core reactivity,
- Performing various measurements with the zero method, covering the 0-4 $W.g^{-1}$ heating range,
- Measurement of separated distributions (nuclear heating or thermal neutron flux),
- Measurement of simultaneous distributions (nuclear heating and thermal neutron flux),
- Test of all possibilities offered by the HMI system to set the parameters before the scanning (scan step from 88 to 11mm, moving-up or moving-down, waiting time at each step, data acquisition for a long time…).

All these tests required, for the only CALMOS-2 device, the total following durations:

- 3 monitored cycles (F282, F283 and F284),
- A total 14 hours recording time of the start-up phase, from 0 to the nominal power,
- A 74 hours total duration of automatic scanning time, thanks to the specific software and the human machine interface (HMI),
- More than 19 days monitoring time of the residual power decay.

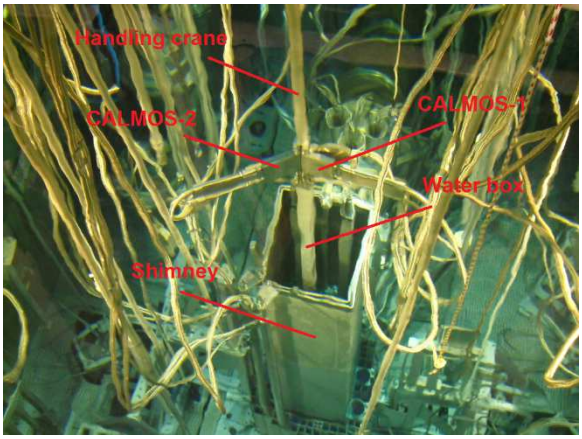


Fig. 19. Moving down of the loaded water box, equipped with both CALMOS devices, with the handling crane inside the 64 experimental location.

Fig 19 shows the F284 loading phase (with CALMOS devices in the same water box which is being put into place but not completely inserted yet), while Fig.20 shows a top view of the final configuration after the loading completion, just before reactor start-up.

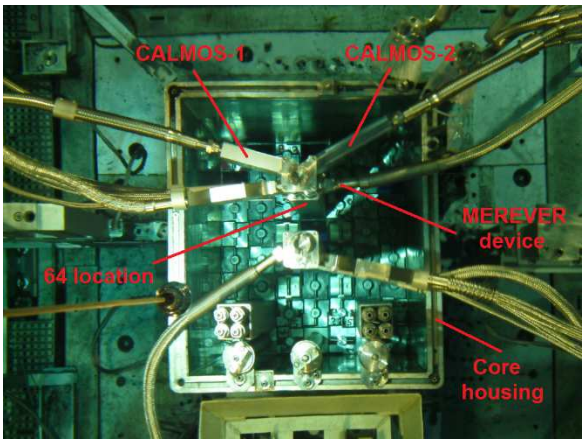


Fig. 20. Loading configuration of the core during the last F284 OSIRIS cycle. Both CALMOS prototypes are located side-by-side in the incore 64 experimental location (respectively 64NW and 64 NE positions). In addition, the MEREVER device dedicated to thermal flux measurement is in the same location in 64South-East position.

12. Establishment of the nuclear heating profile inside the core

To illustrate the way of performing the heating profile in the core, Fig. 21 shows an example of signal acquisition in the 24North-East location. On the same graph are plotted at each scan step (here 48 mm) ΔT sample, ΔT reference and their difference ΔΔT, from which the nuclear heating is calculated (2). In case of CALMOS-1, the lowest position (under -139 mm) is not accessible with the sample cell, whereas above the core the highest position (above +906 mm) is not accessible with the reference cell, due to the probe configuration made up of a cell superimposed to another one with a 95 mm separation distance (88mm for CALMOS-2). Magnification scale (on right) permits to observe variations above the core.

In Fig. 22 are plotted together normalized values (to unity) of ΔT sample, ΔT reference and ΔΔT the difference among them. If the only quantity representative of the energy deposit in the sample graphite is ΔΔT, the relative distribution can be obtained by each ΔT measurement (sample, reference or their difference).

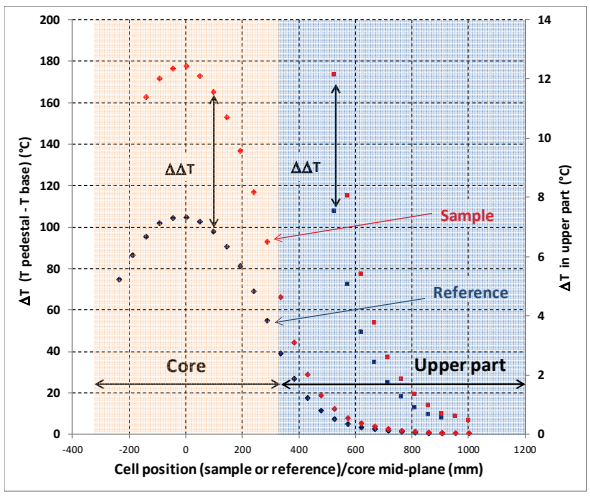


Fig. 21. Example of signals acquisition in 24North-East location of the core. Temperatures of ΔT sample and ΔT reference are recorded along the 1150mm total stroke. The core fissile height is between +/- 320 mm vs the core mid-plane (zoom in right scale).

The three distributions are very close to each other. That is an important remark. That allows deducing the absolute distribution of heating in the reactor with only one measurement at a given altitude and with one of the three possible relative distributions.

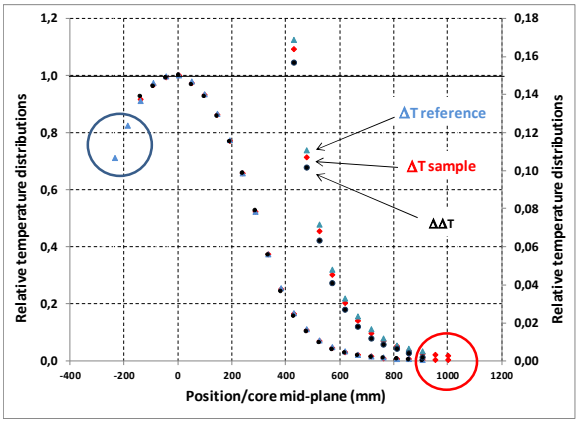


Fig. 22. Distributions normalized to unity of ΔT sample, ΔT reference and ΔΔT in the 24North-East location of the core obtained by CALMOS-1 (zoom in right scale).

On the other hand, that allows extending the heating profile on highest and on lowest altitudes (blue and red circles in Fig. 21), for which it is impossible to measure the ΔΔT quantity due to the two superimposed cells configuration (Fig. 2). The highest altitudes are inaccessible to the empty cell, whereas lowest attitudes are inaccessible to the sample one.

13. Test of the zero method and evaluation of the nonlinearity

The "zero method" is the research of the equilibrium between cells, by balancing the nuclear energy deposit in the sample by a joule effect in the reference one. This method is considered as a reference (illustrated in § 4.2). However, it cannot be used in routine to establish the complete heating distribution inside the core, due to the time required for reaching the temperatures equilibrium. Secondly, it is only applicable in upper part of the distribution where heating levels remain under around 4 $W.g^{-1}$, due to the maximum current intensity (2 A) applicable to heater wires. Nevertheless, as considered as the best approach of an absolute measurement, it enables to confirm results obtained by the calibration curve. In addition, the zero method is a way to study the loss of linearity as the heating rate increases. Therefore, an intensive use of this procedure was made during the 2015 measurement campaign of CALMOS-2. Fig. 23 gathers 21 heating measurements obtained by both calibration and zero methods on the 0-4 $W.g^{-1}$ range. All measurements are obtained by the 4-wire technique leading to a very accurate power measurement (§ 4.2). Note that the zero method can require a significant measurement time because, close to the equilibrium, after each power adjustment we are dependent to the calorimeter time constant.

Fig. 23 gathers all results. The observed dispersion at very low heating rate (9 measurements under 700 $mW.g^{-1}$), is not considered as relevant. However, the figure shows that the discrepancy is within 2% up to around a 2.5 $W.g^{-1}$ heating range. Accounting experimental uncertainties (see § 16), we consider that no loss of linearity is highlighted and both methods are very close to each other up to that point. Beyond, the zero method provides values slightly higher than those obtained by calibration. That leads to a first experimental evaluation of the K_C correction factor to apply in equation (2), but limited to the 0-4 $W.g^{-1}$ range:

$$K_C(E_T) \approx 0.00268\, E_T^2 + 0.00374 E_T + 1 \qquad (5)$$

Therefore, the correction is close to 4% at 3.5 $W.g^{-1}$ and 5 % at 4 $W.g^{-1}$.

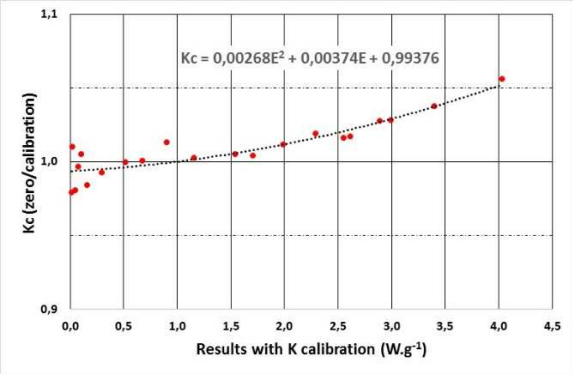


Fig. 23. Results discrepancy between "zero method" and "K calibration" methods up to a 4 $W.g^{-1}$ nuclear heating rate.

The remaining problem is evaluating the loss of linearity beyond 4 $W.g^{-1}$, i.e up to heating rates at the nominal power. That requires a reference measurement on which we can refer to follow accurately the proportional increase of the local power close to the calorimeter vicinity (see § 17.6).

14. Comparison between CALMOS and previous calorimeters

As any device in the core is loaded before the reactor start-up and withdrawn only after shutdown, it is impossible to compare two devices at the same location during the same cycle. Therefore, to qualify the transposition of the previous calorimeters geometry to the CALMOS one, the inter-comparison has been made in the excore area where insertion or removal of devices are allowed when the reactor is operating.

A first comparison was carried out in various excore locations with the second mock-up of CALMOS (very similar to the final geometry) and classical calorimeters. Table 4 shows the inter-comparison with a standard equipment (as described in Fig.1), made at three different locations and at the mid-plane.

Excore location	Calmos (2^{nd} mock-up)	Calor. N°30	Ratio (Calmos/N°30)

	(W/g)	(W/g)	
J1	1.22	1.14	**1.07**
H10	0.96	1.04	**0.92**
H9	1.90	1.67	**1.14**

Table. 4 – Comparison of a previous calorimeter (N°30) and the CALMOS mock-up in excore locations at the core mid-plane.

Despite some differences between measurement systems (aluminum alloys, external diameter, and gas volume), this comparison shows a relative good agreement within 15 % for a heating up to 1.7 $W.g^{-1}$. Nevertheless, this comparison must only retained as an indication.

A global comparison was made also for incore locations.

Incore location	Orientation	5-stage ($W.g^{-1}$)	CALMOS ($W.g^{-1}$)	Ratio (Calm/ 5-stage)
24 South	East West	- 3.55	4.31 -	**1.21**
24 North	East West	- 6.12	5.89 -	**0.96**
44	North-East South-West	7.20 -	- 7.90	**1.10**
64 South	East West	10.7 -	- 9.60	**0.90**

Table. 5 – Comparison betwwen CALMOS-1 and the 5-stage calorimeter for incore locations.

Table 5 brings together some incore measurements, obtained by both the 5-stage calorimeter and CALMOS-1 along different cycles. Unfortunately, like in excore area, the comparison is only indicative:

- The reactor cycle is not the same, leading to a difference in the core loading,
- The location is the same, not the orientation,
- For 44 and 64 locations, measurements with CALMOS-1 are obtained just after the reactor start-up, during the fast evolution of control rods,
- Finally, differences in terms of geometry between both calorimeters are significant, essentially the gas volume and the presence of the external sheath for CALMOS-1.

For the three locations (24North, 44, and 64) the discrepancy does not exceed 10%, but is higher for the 24North location. Despite these differences, a relative good agreement is obtained between the two experimental devices.

15. Comparison with Monte Carlo calculations

15.1 Nuclear heating calculation scheme

To evaluate the nuclear heating in devices irradiated in the OSIRIS reactor, a three-dimensional coupled neutron-photon calculation scheme has been set up. The calculation scheme architecture is presented in Figure 24. It is based mainly on the TRIPOLI-4 Monte Carlo transport code [10, 14, 20, 22] which has been extensively validated against experimental results from neutron flux measurements performed in ex-core and in-core experiments [15, 18, 21]. As shown in Fig. 24, two-step TRIPOLI-4 simulations are needed to estimate the total nuclear heating. The first one is a coupled neutron-photon critical simulation for the calculation of the nuclear heating due to neutrons and prompt photons. The second one is a photon fixed- source simulation devoted for the transport of the fission-product decay gammas. These two main steps need upcoming data: nuclear data which represent the physics of simulations and irradiation data for setting up geometry and compositions of the core. The calculation scheme uses nuclear data from the CEAV5_1.1 library, based mainly on the nuclear data library JEFF3.1.1 [6].

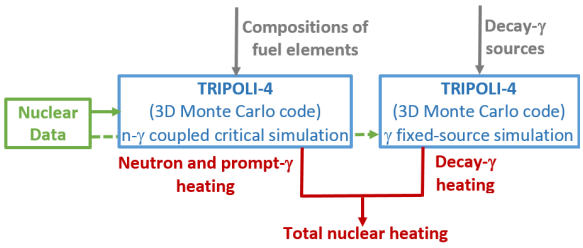


Fig. 24. Nuclear heating evaluation scheme architecture based on TRIPOLI-4 two-step neutron-photon simulations.

The user either gives irradiation data (control rods positions, loading of experimental devices…) or computes them by some deterministic calculation codes, in particular to obtain the isotopic compositions and the decay-gamma sources of the OSIRIS fuel elements.

The five-stage calorimeter (see Fig. 1) and the CALMOS-1 device were modelled thanks to the technical drawings as close as reasonably possible. Figures 25 and 26 show the axial and radial cross sections of the TRIPOLI-4 geometry modelling of the CALMOS device.

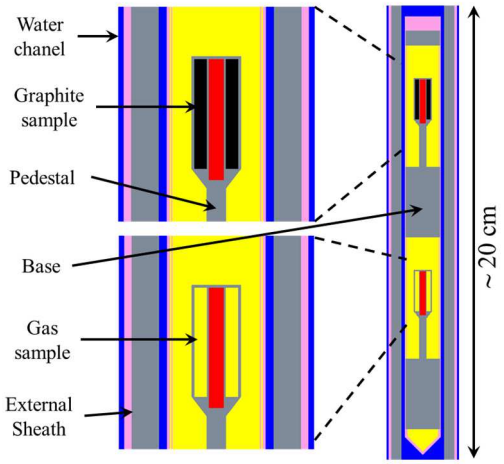
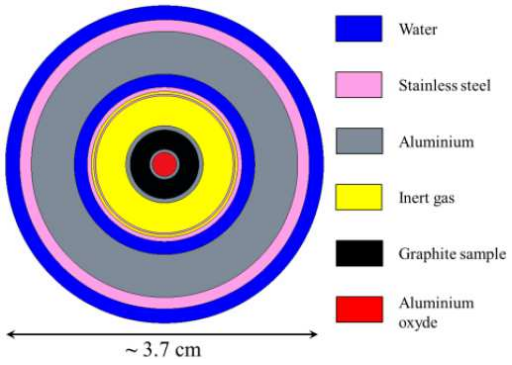


Fig. 25. Axial cross section of a TRIPOLI-4 modelling of the CALMOS-1 device



734

735

736 Fig. 26. Radial cross section of the TRIPOLI-4 geometry modelling of the CALMOS-1 device

737

738 The modelling of the OSIRIS core geometry is also as close as possible to technical drawings. Each fuel plate
739 is modelled in the lattice, control rods can be modeled at their real axial position, and the axial discretization of
740 fuel element compositions can be modified.

741 To ensure Monte Carlo standard deviations less than 1% for all calculated tallies (for fluxes or nuclear heating
742 for neutrons, prompt and decay photons), each TRIPOLI-4 simulation was carried out using one hundred
743 processors during about ten days.

744

745 *15.2 Results*

746

747 Several comparisons between calculations and measurements were performed with the five-stage calorimeter
748 and the CALMOS-1 experimental device when irradiated in different positions and during different cycles of the
749 OSIRIS reactor.

750

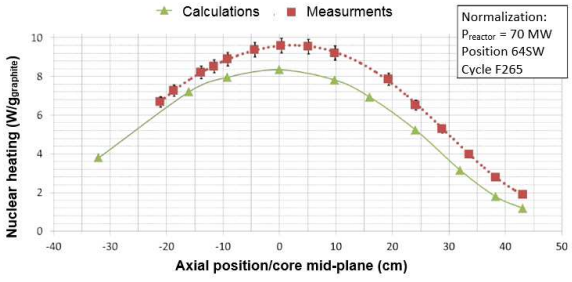


Fig. 27. Axial profile of nuclear heating: calculation-measurement comparison for the CALMOS-1 device (64SW location, cycle F265)

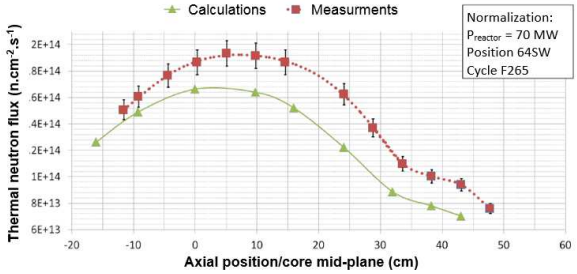


Fig. 28 Axial profile of the thermal neutron flux: calculation-measurement comparison for the CALMOS-1 device (64SW location, F265 cycle).

Figures 27 and 28 show examples of typical calculated and measured axial profiles of nuclear heating (in the graphite sample) and thermal neutron flux (at the rhodium SPND location) for the CALMOS-1 device.

Results shown in these figures correspond to the F265 cycle and the 64 South-West experimental location, normalized at the 70MW rated power.

Globally, we have good consistency between axial profiles of nuclear heating and thermal neutron flux obtained both by calculations and by measurements. However, calculated values systematically underestimate those measured. Discrepancies between calculation and measurements are about -15% at the core mid-plane level. According to measurement uncertainties (see §16), we can consider that the calculated values are close to measurement results within 2σ of measurement. A first possible reason of the observed discrepancies between experiments and simulations could be the lack of knowledge of the exact composition of the fuel elements (determined by preliminary calculations). Another assumption could be a lack in terms of photon production nuclear data. The use of recent nuclear data evaluations such JEFF3.3 or ENDF/B-VIII will be investigated.

The nuclear heating calculation scheme is a useful tool for analysis and understanding. That allowed quantifying a "geometric effect" of 6% in terms of measured nuclear heating, between the five-stage calorimeter and CALMOS, when both devices are irradiated exactly in the same incore position.

Measurements performed by the two calorimeters cannot really be directly compared. This would have required identical irradiation conditions in a same core i.e in terms of core loading and control rods positions (see §14 and Table 5). Therefore, the simulation can be here a good help to perform a fully relevant comparison.

In addition, with the presented calculation scheme, we have access at each component taking part in the nuclear heating in the samples: Neutron energy deposition (about 15%), prompt photon energy deposition (about 65%), and decay photon energy deposition (about 20%). The most part of nuclear heating being due to photons (about 85 %). The contribution of neutrons (essentially fast neutrons above 1 MeV) is not negligible.

16. Uncertainties evaluation

16.1 Nuclear heating measurement

Uncertainties associated to nuclear heating measurements are established when the preliminary calibration (2) is used in routine to perform the measurement (use of the K coefficient). However, such evaluation is made accurately only for the 0-4 $W.g^{-1}$ heating range, for which the zero method could be taken as reference. In that range, the K_C coefficient defining the loss of linearity could be evaluated quite precisely thanks to the 4-wire technique measurement (§ 13). We can consider that the K calibration, the $\Delta\Delta T$ temperature difference and the K_C correction coefficient of (2) are independent:

- The uncertainty associated to K depends on the cell slopes determination made during the preliminary calibration ($°C.W^{-1}$). It is evaluated at 3.8 % at one standard deviation (1 σ) and is independent of the heating level,
- The $\Delta\Delta T$ value comes from the measurement of four temperatures. The uncertainty of each thermocouple (calibration certificate) and those coming from the temperature measurement device, lead to total uncertainties decreasing with $\Delta\Delta T$ rise: 12 % for 5 °C, 5.5 % for 11 °C and 1.9 % for 42 °C $\Delta\Delta T$ (1 σ),
- Kc is evaluated thanks to the zero method and the CAST3M Finite Element Model [28]. The only experimental process is kept in the present evaluation. Despite of the low measurements we could perform in the core, obtained points fit well with the K_C curve in Fig. 23. An analytical approach allows assessing for Kc a global uncertainty to 2 % (1 σ).

Heating $W.g^{-1}$(graphite)	0.5	1	2	4
σ E_T/E_T at 1 σ (%)	12.7	7.0	5.4	4.7

Table 6 – Uncertainties on heating measurements when deduced from the calibration and up to a 4 $W.g^{-1}$ heating rate

Therefore, if the measurement is made with the preliminary calibration and within a 0 to 4 $W.g^{-1}$ range, expected uncertainties are those of Table 6, as a function of the heating rate. Beyond a 4 $W.g^{-1}$ heating rate, the number of available measurements did not allow to assess the definitive associated uncertainty. However, it is expected to be no less than 15 % (1 σ) at 12 W.g-^{1}.

16.2 Conventional thermal neutron flux

Measurement of the thermal neutron flux thanks to the specific rhodium SPND requires to suppress the epithermal response of the emitter (See § 7). That is the preliminary step to deduce the thermal neutron flux from the measured current. Therefore, the axial distribution of the epithermal flux/thermal flux ratio has been calculated by the TRIPOLI-4 Monte Carlo for the four typical experimental locations inside the core, i.e 24South, 24North, 44, and 64 (sub-locations for central 44 and 64 locations do not need to be distinguished in terms of spectra). The epithermal index was calculated for all accessible altitudes with the calorimeter taking into account the real geometry (sensor + cooling water layers + external sheath), the rods position and the actual core loading. Therefore, the following terms are taken into account for the uncertainty evaluation:

- The calculated epithermal index by TRIPOLI4,
- The thermal sensitivity of the rhodium SPND,
- The measured intensity delivered by the SPND.

Finally, the global uncertainty associated to the conventional thermal flux measurement by this rhodium SPND, in CALMOS-2 configuration, is 8 % at 1 σ [17].

17. Characterization of the OSIRIS incore radiation field thanks to CALMOS devices

17.1 Comparison of heating and thermal flux profiles in the core

The probe allows measuring separately the nuclear heating, the thermal neutron flux or both at the same time. Fig. 29 shows an example with 32 simultaneous measurement points, heating and thermal flux, performed in the 44NorthWest location during the F283 cycle with CALMOS-2, which allows observing behaviors of both quantities along the scanning height (distributions normalized to unity).

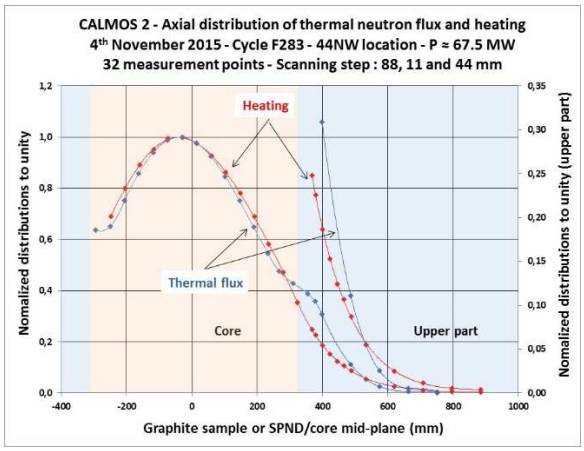


Fig.29 – Simultaneous measurement of heating and thermal neutron flux in the 44North-East location. Values are normalized to unity.

Fig. 29 shows that in the middle part of the core, distributions of heating and neutron flux have roughly the same shape. However, differences of behavior are measured above:

- At the core-moderator transition area centered around +320 mm/mid-plane, we observe a significant rise of thermal neutron flux (slope break), whereas this transition has no effect on the nuclear heating evolution,

- Above the core (zoomed part on right scale of Fig. 29) the heating attenuation is quite different from the thermal flux one. The thermal flux decreases faster than the heating, with a measured ratio of 2 each 40 mm against 80 mm for heating.

17.2 Fine analysis of thermal neutron flux behavior at the core-moderator transition

Fig. 30, which relates to the only thermal flux in absolute values, shows the possibilities offered by the HMI automatic displacement system, allowing to refine deeply the obtained profiles for given areas in the total stroke. At the core-moderator transitions (here in the upper part around +320 mm/mid-plane), the scan step has been reduced to the 11 mm minimum value, detailing the slope break in the thermal flux evolution.

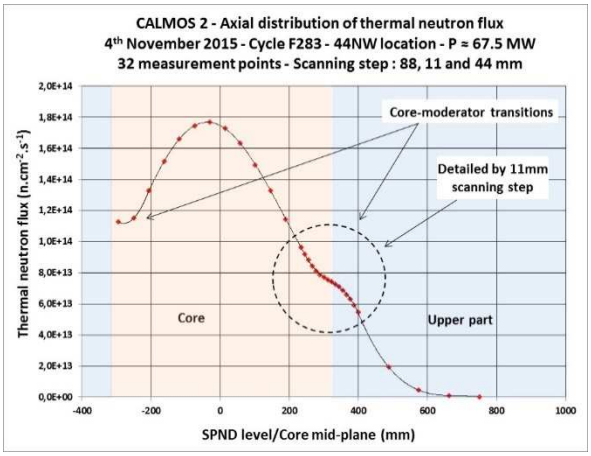


Fig.30 – Measurement of the thermal neutron flux in the 44 North-East location. Detail of the distribution at the core-moderator transition.

17.3 Checking of consistency between both CALMOS devices responses

To check the consistency between CALMOS-1 and CALMOS-2 prototypes, both devices were loaded side-by-side (37 mm distance) in the two north positions of the 64 location during the F284 cycle (Fig. 31). Distributions of nuclear heating and thermal neutron flux were obtained with each device, but operated separately, to avoid any influence on each other. During the scans, made at the 70 MWth nominal power, among the four control rods surrounding the location, only BC3 (in brown) in the south part of the core is in operation and moving in the lower part of its stroke. Such configuration allows approximating same irradiation conditions in north part of the 64 location. Fig. 31 illustrates also the CALMOS configuration with regard to the control rod in operation.

Fig. 31 shows that heating profiles are almost identical, with a slight discrepancy in the mid-plane region in which the CALMOS-2 signal (red curve) is around 3 % higher.

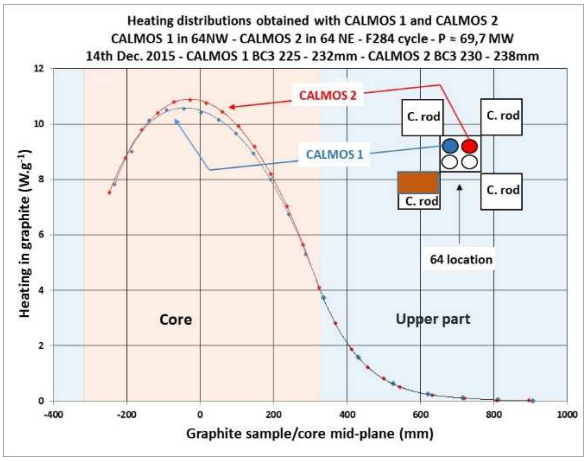


Fig. 31 – Distributions of nuclear heating obtained with both prototypes located in the 64 North location

Such results show that both devices give coherent responses in spite of a significant difference between sensitivities (K calibration discrepancy is 16.6 % between each other).

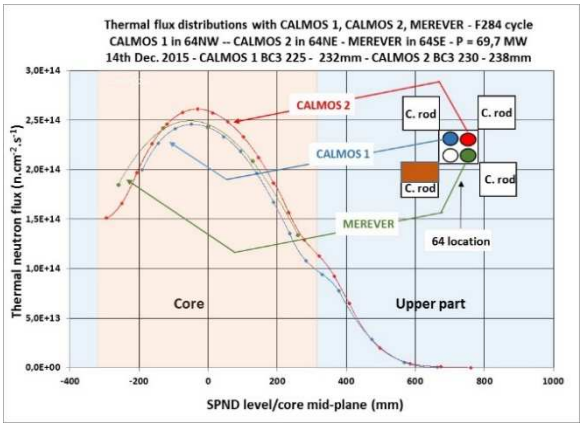


Fig. 32 – Distributions of the thermal neutron flux obtained in 64 location with CALMOS-1 (blue) CALMOS-2 (red) and the MEREVER device (green) equipped with standard rhodium SPNDs

The comparison made for the thermal neutron flux is illustrated in Fig. 32. At mid-plane, measurements by CALMOS-2 (red curve) are also higher around 6 % than CALMOS-1 (blue curve). However, conversely to the heating, we note a thermal flux in CALMOS-1 remaining lower even in the fissile-moderator transition (brown-blue transition on Fig. 32).

In addition, a static device called MEREVER is located also in the same 64SE location (in green). Used for many years in the OSIRIS reactor for thermal flux measurements and qualified, it is instrumented with 10 rhodium standard SPNDs (50 mm emitter length) inside an aluminum rod and allows to plot the flux profile with 5 axial measurements points covering +/-260 mm/mid-plane. In comparison with those obtained with CALMOS devices, we observe that profiles are very similar, except for low altitudes under the mid-plane (green curve), demonstrating that the thermal neutron flux at the MEREVER position is influenced by the rod position, closer to this device.

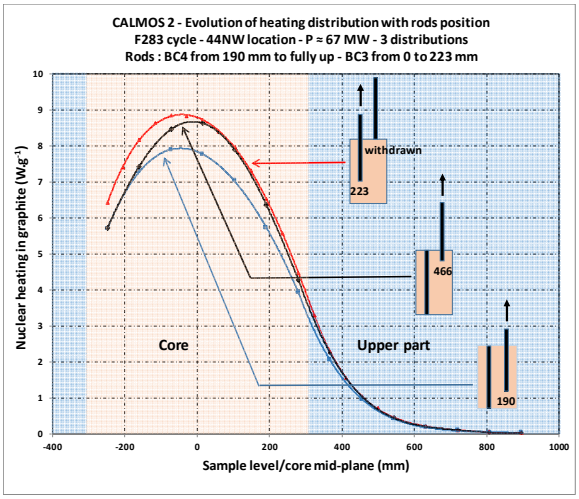
The global consistency in thermal flux measurement found between CALMOS and MEREVER devices, shows that the 10mm short emitter SPND, especially developed for the CALMOS program, is qualified.

895 *17.4 Surveillance of the heating evolution during a reactor cycle*

896

897 To follow the evolution of the heating distribution along the entire reactor F283 cycle, the CALMOS-2 device
898 is placed inside the 44North-West location. Eight different scans are successively performed (reactor power
899 unchanged), spread from the beginning of the cycle to the reactor shutdown.

900



901

902

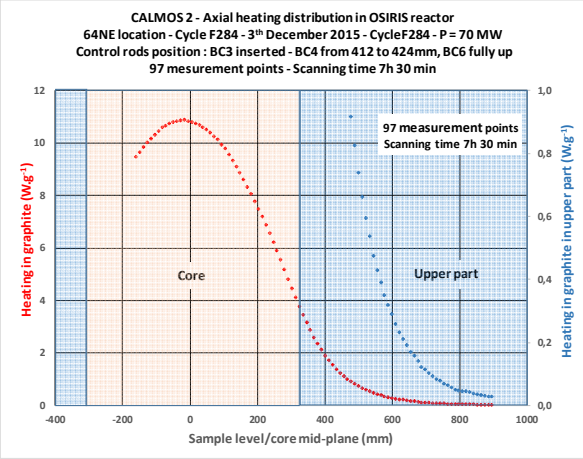
903 Fig. 33 – Follow-up during the whole F283 reactor cycle of the nuclear heating distribution obtained with the CALMOS-2 device placed in the 44
904 North-West location. Three distributions corresponding to three representative control rods positions along the cycle.

905

906 The three most relevant distributions obtained are plotted in Fig. 33, well representative of the whole control
907 rods evolution during the cycle going from the position “rods inserted” (blue curve) to the rods position at
908 shutdown time, with one rod completely extracted (red curve).

909 The complete recording along the cycle permits to measure at this location, not only a 12 % increase of the
910 heating rate at the core mid-plane, but also to observe and to measure the axial displacement of the position of the
911 maximum flux plane (moving from -40 mm, 0 and moving down again -40 mm/MP at shutdown time).

912 Such information is of major importance to predict the total heat deposition in any experimental device in the
913 core.
914
915 *17.5 Heating distribution with very high definition*
916
917 To measure a relevant distribution in the core (heating or neutron flux), the control rods axial displacement
918 (rise movement) must be very short during the whole scan duration, i.e involving a negligible effect on measured
919 distributions. That can be the case only at mid-cycle, because rods are in the middle of their mechanical stroke,
920 therefore at their maximum efficiency. Fig. 34 shows an example of a complete scanning, covering the whole
921 calorimeter stroke, performed with the 11 mm minimum scanning step, offering the best definition. Taking into
922 account the time response of the calorimeter (2min 30s), added to the time required to move the probe, the total
923 measurement time is 4min 30s per point. A 7 h 30 min scanning time is required to perform the 97 measurement
924 points necessary to cover the whole calorimeter stroke. That shows the ability of such calorimeter, thanks to the
925 automatic displacement system, to refine the profile definition as deeply as necessary.
926 Obviously, the measurement is a compromise between the definition and the acceptable scanning time. To
927 keep relevant, the modification of the radiation field must be considered as negligible over the total time required
928 to draw its distribution.
929



930

931

932 Fig. 34. Test of the highest definition. Nuclear heating distribution in the 64North-Esat location during the F284 cycle. The whole scanning height is
933 covered by 97 measurements points for a total scanning time of 7 hr 30 min.

934

935 *17.6 Reactor start-up monitoring*

936

937 For monitoring the complete divergence of the reactor during the F284 cycle, the CALMOS-2 calorimeter
938 (sample cell) is placed at the core mid-plane altitude before start-up. The 64-water box loading is as described in
939 Figs. 31 and 32, with CALMOS-2 in 64North-East and the MEREVER device in 64South-Est location, with only
940 a 37 mm distance between both devices. During the reactor power rise, from the divergence to nominal power,
941 the only two BC6 and BC4 control rods are operating. Other rods are either fully up or fully inserted i.e without
942 any effect on the axial heating distribution. Relative positions between these two rods and devices appear in Fig.
943 32.

944 Among the ten rhodium SPNDs inside the MEREVER device, two SPNDs (N°5 and N°6) are side by side and
945 exactly at the core mid-plane i.e very close to the sample cell of the calorimeter. During the power rise, we can
946 make the following assumptions regarding positions of the sample cell and that of these two SPNDs:

- During the power rise, up to around 50 MW, first the BC6 rod is moving up in the upper part of its stroke between 430 and 550 mm, i.e in an area clearly above the mid-plane. Then, the second rod is moving up in the lower part of its stroke, from 50 MW to nominal power, between 0 and 170 mm i.e clearly under the mid-plane. These two areas are far away enough from the core mid-plane vicinity to consider that, in a first approach, there is no significant effect on the flux gradient between 64NE and 64SE positions,
- As there is no change of environment at the mid-plane vicinity (control rods in operation, static position of the CALMOS calorimeter), the spectrum does not change with reactor power i.e the gamma spectrum, the neutron spectrum and the ratio among them remain unchanged.

Such situation allows assuming, and that was the researched objective, that the nuclear heating (CALMOS-2 monitoring) and the thermal neutron flux (MEREVER monitoring) follow the same relative evolution from the divergence to the nominal power. Therefore, signals recorded from N°5 and N°6 SPNDs of the MEREVER device can be taken as reference to monitor the calorimeter linearity from 0 to 70 MW.

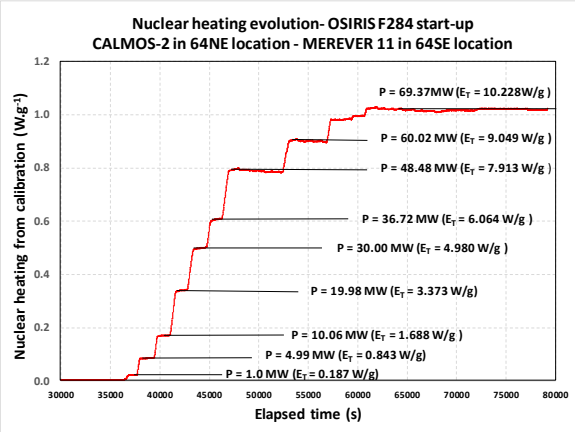


Fig. 35- CALMOS-2 in 64North-East location: Recording of nuclear heating evolution along the F284 reactor start-up from 0 to 69.37 MW. The MEREVER device is in 64South-East location. The reactor power rise is made with 9 steps allowing the recording of stabilized signals.

Fig. 35 shows the evolution of the measured heating (deduced from the calibration) with the CALMOS-2 calorimeter along the whole F284 OSIRIS divergence. Nine steps during the power rise allow to record stabilized signals of the calorimeter and those provided by SPNDs.

The results processing allows deducing a second estimation of the linearity loss for heating measurements up to the nominal power. To do it, the heating measured at 5 MW is taken as reference then, all other measurements are recalibrated thanks to the relative evolution of MEREVER SPNDs. We note that the obtained correction is identical whatever the SPND taken as reference (N°5 or N°6). Fig. 36 shows the deduced experimental evolution of $K_C\,(E_T)$ (ratio between recalibrated and measured values) between 0 and 70 MW i.e covering the 0 to 11 $W.g^{-1}$ heating range:

$$K_C\,(E_T) \approx 0.0006\,E_T^2 + 0.0082E_T + 1 \quad (6)$$

Results show that the correction is not negligible and close to 10 % at 8 W/g and close to 14 % at 10 $W.g^{-1}$.

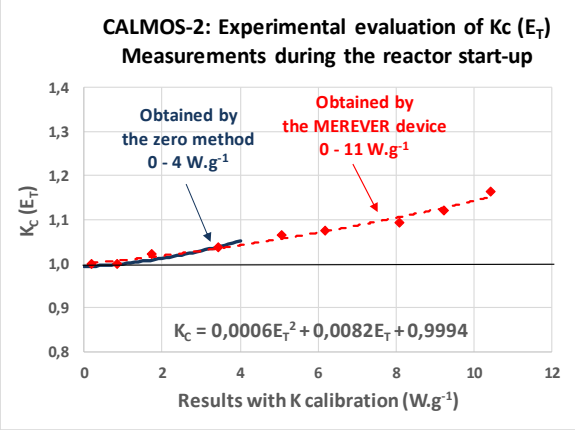


Fig. 36 – CALMOS-2 at the core mid-plane in the 64North-East location: Loss of linearity up to the nominal power during the F284 OSIRIS start-up. Recalibration of heating measuremets thanks to the MEREVER rodium SPNDs in close vicintity.

On the same figure are plotted also, the first experimental evaluation of K_C (E_T) deduced from the zero method comparison (see § 12). Fig. 36 shows that the trend previously obtained, for the correction coefficient limited to a 0-4 W/g heating range, is in correct agreement with these latest measurements.

To reinforce such result, the processing of measured heating levels has been made also with the reactor power taken as reference. In that case, we need to consider that any variation of the reactor global power involves a same relative variation of the local power at the mid-plane vicinity. The same trend is obtained with a correction close to 14 % at 10.4 $W.g^{-1}$ against 15 % found in Fig. 36. Therefore, for nuclear heating measurements obtained from the calibration in CALMOS-2, the K_C expression of (6) is applied.

17.7 Recording of the residual power decay after shutdown

The CALMOS calorimeter has been tested also to follow the residual power decay after the reactor shutdown. Fig. 37 shows a 10 hours recording performed after shutdown at the end of the F283 cycle. Just after shutdown, the residual power drops sharply to almost 10% of the nominal value, before decreasing more slowly. After an 8 hours elapsed time, the measured $\Delta\Delta T$ is only 1.63 °C leading to a residual heating level to around 150 $mW.g^{-1}$. At this time, the reactor procedure requires to stop the primary pumps, involving a change of cooling conditions for the calorimeter, switching from the forced convection to the natural convection regime.

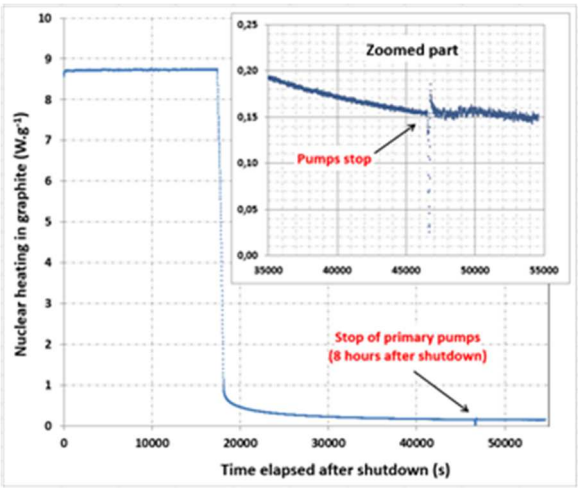


Fig. 37 – Decay of the residual power after the end of the F283 OSIRIS cycle. Recording during 10 hours after shutdown. The signal behaviour before and after the change of cooling regime appears in the zoomed part (upper right corner).

The zoomed part in Fig. 37 (upper right corner) shows that the signal is disturbed at the pump stop and the noise becomes stronger in natural convection. However, the signal decay is still coherent because, after this event, it follows the same slope of decay, demonstrating that the calorimeter remains reliable even in natural convection regime, established inside the water gap between the calorimetric probe and the internal surface of the sleeve. This result is of major importance because that shows that the CALMOS calorimeter keeps its ability to monitor the residual power independently of OSIRIS thermohydraulic conditions.

17.8 Establishment of the core residual power distribution 18 days after shutdown

At the end of the F284 cycle, the monitoring of the power residual decay was extended up to 18 days after the reactor shutdown. At this time, when the CALMOS probe is located at the core mid-plane, the measured $\Delta\Delta T$ is reduced to 0.31 °C leading to a nuclear heating rate of about 29 $mW.g^{-1}$ (C).

Despite this very low signal, a scanning is attempted to establish the axial distribution of the residual power in the core, in 64North-East location, with a step reduced to 22 mm and a 5 min measurement time at each altitude. Fig. 38 shows the obtained recording of ΔΔT raw values. Despite some discrepancies, the nuclear heating distribution is still coherent and measurable.

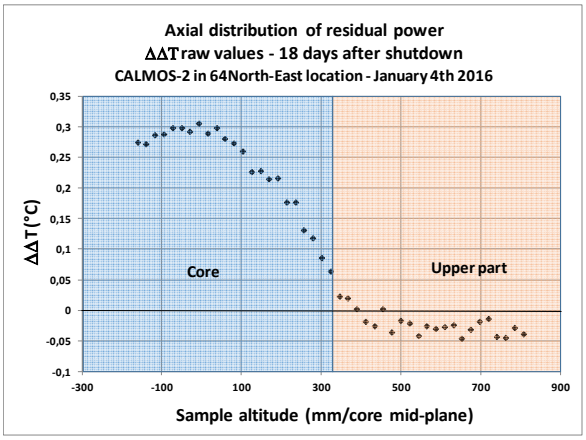


Fig. 38 – Axial distribution of raw ΔΔT values of the CALMOS-2 calorimeter, in the 64NE expertimental location, 18 days after shutdown of the F284 OSIRIS cycle.

We remind that the study of the calorimetric cell response shows clearly that, even though ΔΔT is the only quantity well representative of nuclear heating, the relative distribution can be deduced from each cell ΔT as demonstrated in Fig. 22. Taking advantage of this property, for plotting the complete curve of the final residual power in the core, we retain only the absolute measurement of heating at the core mid-plane. Then, the rest of the distribution is deduced from the relative response of the "Δt sample" showing a much weaker dispersion. Results appear in Fig.39.

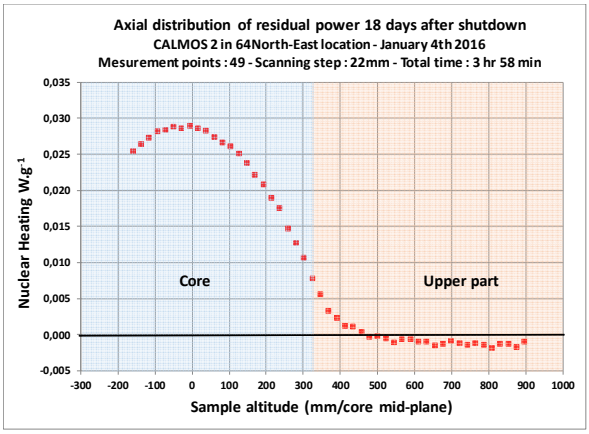


Fig. 39 – Axial distribution of the core residual power, plotted by the CALMOS-2 measurement device 18 days after shutdown of the OSIRIS F284 cycle.

That demonstrates that it is of prior importance, during the manufacturing, to choose the thermocouples accurately to enable the very low ΔT measurements. They must provide the lowest dispersion as possible in a same temperature field (importance of preliminary calibration). Each thermocouple embedded in the cell base ("cold temperature") is calibrated with two reference points, melting ice and boiling of water, whereas each thermocouple embedded in the pedestal ("hot temperature") is calibrated with four references, boiling of water and melting points of Tin (232 °C), Lead (327 °C), and Zinc (420 °C). After selection, the lower the dispersion is, the lower the required correction is (or negligible) for very low heating rates. For the four thermocouples of the CALMOS-2 calorimetric cell, the preselection led to a very low discrepancy among them, measured to 0.2 °C over the 420 °C total range of the calibration.

Obtained results show the ability of the CALMOS device to establish the nuclear heating distribution in the core, from the nominal power up to after 18 days of cooling time after shutdown. Therefore, we can consider that the calorimetric cell offers 3-decade dynamic range.

18. Mutual perturbation between the two CALMOS devices in a same experimental location

Inside an experimental reactor, it is essential to check that the measurement we are performing is relevant. That requires checking that any potential modification in the environment (control rod, experimental device…) does not affect significantly the radiation field we are measuring. That is the case if we want to use the two CALMOS devices in the same water box to characterize the same location. Moving down or moving up the mobile equipment of a system along its main axis can disturb the other one.

During the last F284 cycle, CALMOS-1 and CALMOS-2 were placed side-by-side, respectively in the 64North-West and the 64 North-East locations of the core.

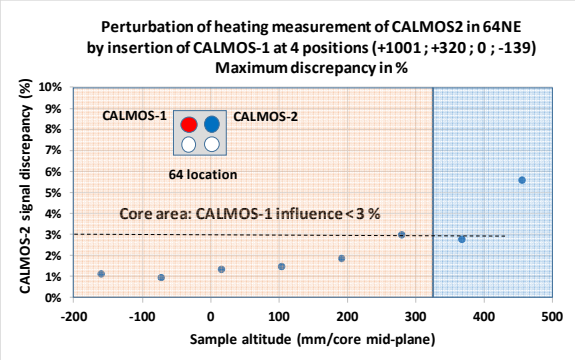


Fig. 40 – CALMOS-2: Discrepancy in nuclear heating measurement among the 4 measurements corresponding to the 4 positions of the CALMOS-1 probe insertion in the core.

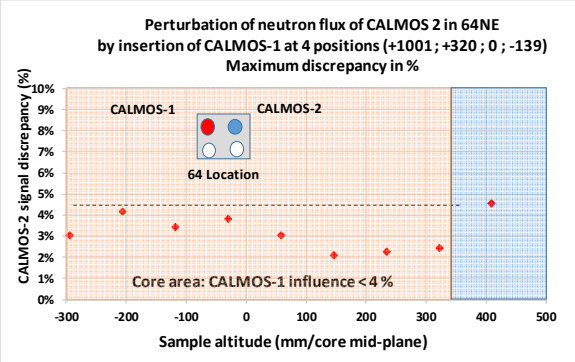


Fig. 41 – CALMOS-2: Discrepancy in thermal neutron flux measurement among 4 measurements corresponding to 4 positions of the CALMOS-1 probe insertion in the core.

Four successive complete scanning were performed with CALMOS-2 (nuclear heating + neutron flux measurements, 88mm scan step each) for four fixed positions of the CALMOS-1 calorimetric probe, corresponding to the rest position (+1001mm), the entrance of the core (+320 mm), the core mid-plane (0mm), and at the bottom (-139 mm). These four positions are representative of the potential perturbation.

Figs. 40 and 41 gather all maximum measured discrepancies, evaluated at eight altitudes of CALMOS-2 calorimeter, for both heating and neutron flux measurements. Results show that, inside the core, the maximum perturbation involved by the presence of the CALMOS-1 probe in CALMOS-2 vicinity remains very low, respectively less than 3 % for heating measurement and less than 4% for the thermal neutron flux. Considering experimental uncertainties, such results led us to assume that, in first approximation, any scanning performed by one displacement system does not disturb the measurements acquisition carried out by any other similar device, for both nuclear heating or for thermal neutron flux measurements. Both devices can work together independently.

19. Conclusion

From the first idea in 2002 to the completion of a real qualified measurement prototype suited to an MTR reactor, followed by the comprehensive analysis of obtained results, the CALMOS R&D program took place over a period of 15 years. The development and the qualification of the whole measurement system required a succession of thermohydraulic, neutron, and mechanical studies. Among them, the modelling of the calorimetric probe, answering to OSIRIS incore thermohydraulic conditions, permitted to design a cell geometry well suited to nuclear heating rates inside the core. Two mock-ups tested in the excore area allowed to validate the measurement protocol for this innovative superimposed geometry. Then, the transposition to incore measurements needed the development of a specific displacement system to obtain axial nuclear heating distributions inside the core while ensuring the cooling conditions of the probe and matching with OSIRIS safety requirements. The whole measurement campaign in real incore conditions by both CALMOS devices ran from 2013 to 2015, covering 11 reactor cycles, around 22 days each.

About the calorimetric probe working, the main results are as follows:

- Using the zero method, almost independent of the calibration phase, allows reducing the number of assumptions in the heating measurement process. The most important improvement brought in the last version is the implementation of the 4-wire technique in the reference cell, which allows suppressing any assumption about the heater element ageing. That enables to reduce the associated uncertainty to heating measurements at 4.7 % at 1σ for a 4 $W.g^{-1}$ (C) heating rate,
- The entire absolute axial distribution in the core can be obtained by performing a single absolute measurement at a given altitude, the rest of the curve is deduced thanks to the relative response of any of the cells,
- The zero method is used as a reference measurement for the probe non-linearity assessment. Determination of the cells slope in $°C.W^{-1}$ shows that the response is almost linear within a 0-5 $W.g^{-1}$ heating range, with a measured discrepancy not exceeding 4 %,

- The global sensitivity has around a 3-decade dynamic range, offering the possibility not only to follow the core residual power up to 2 weeks after shutdown, but also after this cooling time to draw its axial distribution.

The CALMOS-1 device has been tested during ten reactor cycles. Despite the short irradiation campaign of the CALMOS-2 upgraded version, carried out during the last three cycles of the OSIRIS reactor due to its final shutdown scheduled in December 2015, many tests were performed in different core conditions. That highlighted the various possibilities offered by the new displacement system when associated with the complete automatic driving system to characterize the incore radiation field. Among major results, we note:

- The automatic probe mobility, programmed through a Human Machine Interface thanks to a specific software, allows obtaining very well defined profiles both for nuclear heating and for thermal neutron flux measurements. The scanning step and partial and/or total measurement times can be adjusted as required, focused on given target regions and to the reactor conditions in order to keep a relevant measurement with regard to the control rods evolution,
- The programming of measurement sequences helps a lot in monitoring the radiation field evolution throughout the reactor cycle, because it can be adapted to reactor conditions,
- For the most critical situation, a CALMOS device closer as possible to the control rod in operation, the complete withdrawal of the mobile equipment from its external sheath induces a 45 pcm positive reactivity on the core. Therefore, the adopted displacement speed of 1 $mm.s^{-1}$ in the core involves a reactivity effect less than 0.1 $pcm.s^{-1}$, fully compatible with reactor control rules.

However, the global feedback of the CALMOS program leads us to some improvement perspectives. In that program, the main purpose was to obtain a calorimeter answering to a very large nuclear heating range, ranging from 13 $W.g^{-1}$ at the core mid-plane at nominal power to the residual heating at 1 m above the core. Therefore, the sensitivity was a compromise. It must be high enough for a measureable $\Delta\Delta T$ in the lower part of the heating

range, but sufficiently low at high level to limit absolute temperatures in the cell, because leading to heat losses by radiation and conduction in gas. Therefore, in the upper heating range, the loss of the linearity is significant. So, as main prospect, another design would be optimizing the geometry so as to limit the sensitivity, therefore the maximum temperature of inner walls inside the cell, to suppress as drastically as possible heat losses by radiation, which are very difficult to assess by calculation and to suppress in the design.

Secondly, even though it cannot be used in routine for establishing any axial distribution, results showed the importance of the zero method, considered as the best approach of an absolute measurement. That leads to the second major improvement, which would be to design a heater element able to simulate the energy deposit up to highest heating levels in the core, to perform an absolute measurement for assessing more accurately the loss of linearity when using the calibration coefficient.

The intensive use of CALMOS-2 in the core, cumulating a total 70 hours automatic scanning time, has demonstrated its reliability for OSIRIS in-core conditions up to a 12 $W.g^{-1}$ heating rate and up to a 2.5 x 10^{14} $n.cm^{-2}.s^{-1}$ thermal neutron flux. While meeting the reactor safety requirements, the CALMOS device becomes an operational equipment suited to the surveillance and the qualification of the incore radiation field in an MTR reactor, a key data for the dimensioning and the surveillance of any experimental device irradiated inside.

Acknowledgments

This R&D program was carried out in the framework and with the financial support of the MCIS/INSNU project of CEA/DEN. Authors wish to thank the DEN/DER/SPESI and SRJH services of CEA/Cadarache for their support, and the LIMMEX joint laboratory between CEA and Aix-Marseille University for fruitful and constructive discussions along this R&D program.

The constant support of the OSIRIS operating personnel from CEA/DEN at the Saclay center was crucial for performing irradiation campaigns inside the reactor.

Finally, authors wish to address special thanks to Valérie Lepeltier, Véronique Clouté-Cazalaa and Jean-Marie Guyot, Romain Illiaquer, Eric Bouard, Jacques Bubendorff and Cedric Courteaux from the CEA/DEN of the

Saclay center for their help through their respective specialties, without which we could not have conducted this research program.

References

[1] F. Ayela, H. Derrien "The development of an electrically compensated differential calorimeter for the measurement of in-pile heat evolution". Technical Report CEA-R-2190, 1962.

[2] IAEA, "International Intercomparison of Calorimeters", Report N° 128, 1970.

[3] M.S. Kim, S.Y. Hwang, H.S. Jung, and K.H. Lee, "Measurements of Nuclear Heating Rate and Neutron Flux in HANARO CN Hole for Designing the moderator cell of cold neutron source." Korea Atomic Energy Research Institute. Proceedings of IGORR, (2005).

[4] H. Carcreff, A. Alberman, L. Barbot, F. Rozenblum, D. Beretz and Y. K. Lee, "Dosimetry Requirements for Pressure Vessel Steels Toughness Curve in the Ductile to Brittle Range", J. of ASTM International (JAI), Vol. 3, Issue 3, (Mar., 2006).

[5] Y.K. Lee and F. Malouch, "Analysis of OSIRIS In-Core Surveillance Dosimetry for GONDOLE Steel Irradiation Pragram by Using TRIPOLI-4 Monte Carlo Code", 13th International Symposium on Reactor Dosimetry (ISRD13), Akersloot, Netherlands, May 21-25, 2008.

[6] Santamarina A., Bernard D., Blaise P., Coste M., Courcelle A., Huynh T.D., Jouanne C., Leconte P., Litaize O., Mengelle S., Noguère G., Ruggieri J.M., Sérot O., Tommasi J., Vaglio-Gaudard C., Vidal J-F., "The JEFF-3.1.1 Nuclear Data Library, JEFF Report 22, Validation Results from JEF-2.2 to JEFF-3.1.1," NEA No. 6807, OECD/NEA Edition 2009.

[7] H. Carcreff, Patent N° FR 1060068, December 3, 2010.

[8] H. Carcreff, "CALMOS : Innovative device for the measurement of nuclear heating in material testing reactors". Journal of ASTM International (JAI , Volume 9, Issue3, March 2012.

[9] H. Carcreff, V. Clouté-Cazalaa, and L. Salmon, "Development, calibration and experimental results obtained with the innovative calorimeter (CALMOS) for nuclear heating measurements", IEEE Trans. Nucl. Sci.,vol.54, no.4, pp. 1369-1376, Aug.2012.

[10] F. Malouch, “Development and Experimenatl Validation of a Calculation Scheme for Nuclear Heating Evaluation in the Core of the OSIRIS Material Testing Reactor”. Journal of ASTM International (JAI), Volume 9, Issue 4, April 2012.

[11] J. Brun, and coll, “Numerical and Experimental Calibration of a Calorimetric Sample Cell Dedicated to Nuclear Heating Measurements”, IEEE Transactions on Nuclear Science, Vol.59, N°.6, Dec 2012.

[12] F. Lopez “Calculs d’indice épithermique dans le dispositif CALMOS pour m’interprétation du signal collectron dans et au-dessus du coeur du réacteur OSIRIS” note CEA/DEN/DM2S/SERMA/LPEC/NT/13-5545/A. Dec.2013.

[13] J. Brun, C. Reynard-Carette, A. Lyoussi, C. De Vita, M. Carette, M. Muraglia, D. Fourmentel, P. Guimbal and J.F. Villard. “ Comparison of the Thermal Response of Two Calorimetric Cells Dedicated to Nuclear Herating Measurements during Calobration”. Advancements in Nuclear Instrumentation Measurements Methods and their Applications (ANIMMA-2013), Marseille, 23-27 June 2013.

[14] "TRIPOLI-4, The Monte Carlo particle transport code of CEA", http://www.cea.fr/nucleaire/tripoli-4

[15] A. Péron, F. Malouch, C.M. Diop. A. Péron, “Simulation and Comparison of the Calorimeters Measuring the Nuclear Heating in the OSIRIS Reactor, with the TRIPOLI-4 Monte-Carlo Code”, IEEE Transactions on Nuclear Science, Year: 2015 , Volume: 62 , Issue: 3, Pages: 1218 – 1225

[16] H. Carcreff, L. Salmon, and C. Courtaux, “First In-Core Measurement Results Obtained with the Innovative Mobile Calorimeter CALMOS inside the OSIRIS Material Testing Reactor”, IEEE Transactions on Nuclear Science, Vol.61, N°.4, Aug 2014.

[17] D. Fourmentel, and coll. “Comparison of Thermal Neutron Flux Measured by 235U Fission Chamber and Rhodium Self-Powered Neutron Detector in MTR”. IEEE Transactions on Nuclear Science, Vol.61, N°.4, Aug 2014.

[18] A. Péron, F. Malouch, and C. Diop. “Improvement of Nuclear Heating Evaluation Inside the Core of the OSIRIS Material Testing Reactor”. 15th International Symposium on Reactor Dosimetry (ISRD15), Aix en Provence, May 2014.

[19] J.Brun and coll, « influence of thermal conditions on the response of a calorimeter dedicated to nuclear heating measurements », Sensors, IEEE nov 2014, 1336-1339.

[20] E. Brun, F. Damian, C.M. Diop, E. Dumonteil, F.X. Hugot, C. Jouanne, Y.K. Lee, F. Malvagi, A. Mazzolo, O. Petit, J.C. Trama, T. Visonneau, A. Zoia, Tripoli-4®, CEA, EDF and AREVA Reference Monte Carlo Code, Annals of Nuclear Energy 82, 151-160 (2015).

[21] A. Péron. “Contribution à l’Amélioration des Méthodes d’Evaluation de l’Echauffement Nucléaire dans les Réacteurs Nucléaires à l’aide du Code Monte Carlo TRIPOLI-4”.Rapport CEA-R-6419. Jan, 2016.

[22] F. Malouch, E. Brun, F. Damian, F.X-. Hugot, F. Lopez, D. Mancusi, O. Petit, A. Zoia, Recent Developments in the Tripoli-4® Monte Carlo Code - Applications to Research Reactors, RRFM/IGORR2016, Berlin, Germany (2016).

[23] H. Carcreff, and coll, “First In-Core Simultaneous Measurements of Nuclear Heating and Thermal Neutron Flux obtained with the Innovative Mobile Calorimeter CALMOS inside the OSIRIS Reactor“ IEEE Transactions on Nuclear Science, Vol. 63, N°.5, Oct 2016.

[24] "CAST3Mcode", https://web.archive.org/web/20170913085648/http://www-cast3m.cea.fr/

[25] "euralliage", https://web.archive.org/web/20170913085547/http://www.euralliage.com/

[26] C.Vargel « propriétés générales de l'aluminium et de ses alliages », techniques de l'ingénieur, ref M4661

[27] Rapport d'essai du Laboratoire National d'Essai (LNE). Dossier P164040. Dec 2016.

[28] H. Carcreff, L. Salmon,, V. Lepeltier, J.M. Guyot, E. Bouard, "Simultaneous Measurements of Nuclear Heating and Thermal Neutron Flux Obtained with the CALMOS-2 Measurement Device inside the OSIRIS Reactor". Proceedings of ISRD16. Journal of ASTM International, to be published. May, 2017.